AGU ADVANCING EARTH AND SPACE SCIENCES

AGU Advances

RESEARCH ARTICLE
10.1029/2024AV001373

Toward a Universal Model of Hyporheic Exchange and Nutrient Cycling in Streams

Ahmed Monofy[1], Stanley B. Grant[1], Fulvio Boano[2], Megan A. Rippy[1], Jesus D. Gomez-Velez[1,3], Sujay S. Kaushal[4], Erin R. Hotchkiss[5], and Sydney Shelton[4]

[1]Occoquan Watershed Monitoring Laboratory, The Charles E. Via Jr. Department of Civil and Environmental Engineering, Virginia Tech, Manassas, VA, USA, [2]Department of Environment, Land and Infrastructure Engineering, Politecnico di Torino, Torino, Italy, [3]Environmental Sciences Division, Oak Ridge National Laboratory, Climate Change Science Institute, Oak Ridge, TN, USA, [4]Department of Geology and Earth System Science Interdisciplinary Center, University of Maryland, College Park, MD, USA, [5]Department of Biological Sciences, Virginia Polytechnic Institute and State University, Blacksburg, VA, USA

Peer Review The peer review history for this article is available as a PDF in the Supporting Information.

Key Points:

- Several ubiquitous hyporheic exchange mechanisms can be represented by an exponentially decaying diffusivity
- The reference diffusivity and mixing depth can be calculated from a stream's permeability Reynolds Number and Schmidt Number
- Application to headwater streams reveals how land-use, physics, and biology control nitrate uptake

Supporting Information:

Supporting Information may be found in the online version of this article.

Correspondence to:

S. B. Grant,
stanleyg@vt.edu

Citation:

Monofy, A., Grant, S. B., Boano, F., Rippy, M. A., Gomez-Velez, J. D., Kaushal, S. S., et al. (2024). Toward a universal model of hyporheic exchange and nutrient cycling in streams. *AGU Advances*, *5*, e2024AV001373. https://doi.org/10.1029/2024AV001373

Received 24 JUN 2024
Accepted 26 SEP 2024

Author Contributions:

Conceptualization: Ahmed Monofy, Stanley B. Grant, Jesus D. Gomez-Velez, Sujay S. Kaushal, Erin R. Hotchkiss, Sydney Shelton
Data curation: Ahmed Monofy, Stanley B. Grant
Formal analysis: Megan A. Rippy
Funding acquisition: Stanley B. Grant, Sujay S. Kaushal
Methodology: Ahmed Monofy, Stanley B. Grant, Fulvio Boano, Jesus D. Gomez-Velez
Project administration: Stanley B. Grant

Abstract In this paper we demonstrate that several ubiquitous hyporheic exchange mechanisms can be represented simply as a one-dimensional diffusion process, where the diffusivity decays exponentially with depth into the streambed. Based on a meta-analysis of 106 previously published laboratory measurements of hyporheic exchange (capturing a range of bed morphologies, hydraulic conditions, streambed properties, and experimental approaches) we find that the reference diffusivity and mixing length-scale are functions of the permeability Reynolds Number and Schmidt Number. These dimensionless numbers, in turn, can be estimated for a particular stream from the median grain size of the streambed and the stream's depth, slope, and temperature. Application of these results to a seminal study of nitrate removal in 72 headwater streams across the United States, reveals: (a) streams draining urban and agricultural landscapes have a diminished capacity for in-stream and in-bed mixing along with smaller subsurface storage zones compared to streams draining reference landscapes; (b) under steady-state conditions nitrate uptake in the streambed is primarily biologically controlled; and (c) median reaction timescales for nitrate removal in the hyporheic zone are ≈0.5 and 20 hr for uptake by assimilation and denitrification, respectively. While further research is needed, the simplicity and extensibility of the framework described here should facilitate cross-disciplinary discussions and inform reach-scale studies of pollutant fate and transport and their scale-up to watersheds and beyond.

Plain Language Summary Microbial communities in streambed sediments play a crucial role in the transformation and removal of nutrients and pollutants in streams. A key step in this process is the physical transport of a contaminant from the bulk stream to, and through, the streambed, a process broadly referred to as hyporheic exchange. While myriad physical and biological processes influence the rate of hyporheic exchange in a given setting, in this paper we demonstrate that several ubiquitous hyporheic exchange mechanisms can be represented simply as a one-dimensional diffusion process, where the diffusion coefficient decays exponentially with depth into the streambed. Application of this framework to a seminal study of nitrate removal in headwater streams across the United States provides new insights into how land-use, stream physics, and stream biology collectively influence nutrient transport, transformation, and removal in streambed sediments. By leveraging insights across multiple disciplines into a synthetic whole, the modeling framework presented here should catalyze new interdisciplinary discussions and insights into the role that hyporheic exchange plays in the storage, processing, and removal of contaminants in streams.

1. Introduction

The hyporheic zone is the portion of sediments beneath and alongside a stream where stream water, sediment pore water, and groundwater actively mix (Bencala, 2000; Boano et al., 2014; Cardenas, 2015; Gooseff, 2010; Krause et al., 2011, 2022; Ward et al., 2016). It is an important stream habitat (Coll et al., 2020; Gooseff, 2010; Lewandowski et al., 2019) and a "hot spot" for contaminant removal and nutrient cycling along stream corridors (Grant, Azizian, et al., 2018; Grant, Gomez-Velez, & Ghisalberti, 2018; Hall et al., 2009). These hyporheic zone functions depend critically on the exchange of water, solutes and energy with the stream, a process referred to as hyporheic exchange. Hyporheic exchange is driven by a variety of physical and biological factors, including: (a) variation in the permeability of the streambed (Gomez-Velez et al., 2014; Su et al., 2024); (b) variation in static

Resources: Ahmed Monofy
Software: Ahmed Monofy, Stanley B. Grant
Supervision: Stanley B. Grant, Fulvio Boano
Validation: Ahmed Monofy, Stanley B. Grant
Writing – original draft: Ahmed Monofy, Stanley B. Grant
Writing – review & editing: Ahmed Monofy, Stanley B. Grant, Fulvio Boano, Megan A. Rippy, Jesus D. Gomez-Velez, Sujay S. Kaushal, Erin R. Hotchkiss, Sydney Shelton

and dynamic pressure at the sediment-water interface associated with stream morphology (e.g., riffle-pool sequences (Monofy & Boano, 2021; Tonina & Buffington, 2007; Trauth et al., 2013) and stream meanders (Cardenas, 2009; Ren et al., 2023; Stonedahl et al., 2013)) and flow through and over in-stream obstructions including logs (Huang & Yang, 2023; Sawyer et al., 2011) and bedforms (e.g., ripples and dunes (Cardenas et al., 2008; Hester et al., 2013)); (c) dynamic geomorphic processes, such as the bedform migration (Ahmerkamp et al., 2015; Boano et al., 2013; Ping et al., 2022; Shimony et al., 2023); (d) biological processes (e.g., irrigation across the sediment-water interface by macro infauna (Liu et al., 2022; Shrivastava et al., 2021) and flow through bull trout and salmon redds (Baxter & Hauer, 2000; Bhattarai et al., 2023)); and (e) stream turbulence which controls the rate at which mass and energy are mixed vertically through the water column to the sediment-water interface (Grant, Gomez-Velez, & Ghisalberti, 2018) and, if the streambed sediments are sufficiently permeable, the rate of mixing within sediment pore fluids as well (Azizian et al., 2017; Bottacin-Busolin, 2017; Y. Chen et al., 2021; Chandler et al., 2016; Grant, Gomez-Velez, & Ghisalberti, 2018; Grant, Gomez-Velez, et al., 2020; Roche et al., 2019; Voermans et al., 2017, 2018). While each of these exchange mechanisms can be studied and mathematically modeled in isolation, the development of simple and generalizeable frameworks for modeling reactive solute transfer across the sediment-water interface by hyporheic exchange remains a significant challenge.

One promising approach along these lines represents the vertical transport of solutes across the sediment-water interface as a one-dimensional diffusion process, where the magnitude of the diffusion coefficient, or effective diffusivity D_{eff} [L^2 T^{-1}], and its variation with depth y [L] into the streambed are emergent properties of the physical and biological processes responsible for hyporheic exchange in a particular setting (Bottacin-Busolin, 2017). For example, hyporheic exchange by bedform pumping—the laminar flow of water through ripples and dunes—can be equivalently represented as either a two- or three-dimensional advective transport problem (Elliott & Brooks, 1997a; Packman et al., 2004) or as one-dimensional diffusion. In the latter case, the effective diffusivity at the sediment-water interface, $D_{\text{eff},0}$, is a dispersion coefficient that depends on the bedform wavelength λ [L], sediment porosity θ [-] and a characteristic pore-scale velocity u_m [LT^{-1}]: $D_{\text{eff},0} \propto \lambda u_m/\theta$ (Elliott, 1991). The pore-scale velocity captures the influence of the sediment's hydraulic conductivity K_h [LT^{-1}] and the pressure head drop across the lee and stoss sides of the bedform h_m [L]: $u_m \propto K_h h_m/\lambda$ (Elliott & Brooks, 1997a). Because the advective flow field responsible for bedform pumping decays exponentially with depth into the streambed over a length-scale roughly equal to the bedform wavelength, λ (Elliott & Brooks, 1997a), the magnitude of the effective diffusivity also decays exponentially with depth (Grant, Monofy, et al., 2020). Alternatively, if the diffusivity is assumed to be invariant with depth, the magnitude of the effective diffusion coefficient for bedform pumping may appear to vary with time as solutes enter progressively deeper regions of the streambed where the intensity of mixing is reduced (Marion & Zaramella, 2005).

Similarly, turbulent and dispersive mixing across flat porous beds can be represented by an effective diffusivity that decays exponentially with depth (Chandler et al., 2016; Grant, Gomez-Velez, et al., 2020). In this case, the magnitude of the effective diffusivity at the sediment-water interface (i.e., at $y = 0$) depends on the so-called permeability Reynolds Number, $Re_K = \sqrt{K}u_*/\nu$, where K [L^2] is the sediment permeability and u_* [LT^{-1}] and ν [L^2 T^{-1}] are the shear velocity of the stream and the kinematic viscosity of water, respectively: $D_{\text{eff},0} \propto Re_K^b$. The shear velocity is a measure of ambient turbulence in a stream, and is defined as the square root of the friction (or more formally, shear stress) exerted by the stream on the streambed, τ_w [ML^{-1} T^{-2}], divided by stream water density, ρ [M L^{-3}]: $u_* = \sqrt{\tau_w/\rho}$ (Grant & Marusic, 2011). The magnitude of the exponent b [-] ranges from $b \approx 2.5$ when mixing across the sediment-water interface is dominated by turbulent diffusion ($0.01 \leq Re_K \leq 1$) to $b \approx 1$ when mixing is dominated by turbulent dispersion ($Re_K > 1$) (Grant, Gomez-Velez, et al., 2020; Voermans et al., 2018). Interestingly, the dispersion coefficient discussed above for bedform pumping can also be written in terms of the permeability Reynolds number: $D_{\text{eff},0} \propto Re_K^2$ (Grant, Monofy, et al., 2020). Thus, at least two ubiquitous mechanisms for hyporheic exchange in streams—bedform pumping and turbulent diffusion/dispersion—can be parsimoniously represented as a one-dimensional diffusion process with an effective diffusivity that declines exponentially with depth into the streambed. Further, in these two cases the magnitude of effective diffusivity at the sediment-water interface, $D_{\text{eff},0}$, depends on the fundamental balance between the permeability length-scale of the streambed sediments, $\sqrt{K}$, and the inner length-scale of the stream's turbulent velocity boundary layer, ν/u_*, as embodied in the permeability Reynolds number, Re_K.

The above insights, which are gleaned primarily from laboratory flume experiments and multi-physics modeling studies, are also consistent with field measurements of solute transport and hyporheic exchange in streams. For example, Bottacin-Busolin (2017, 2019) have shown that solute breakthrough curves measured during field tracer experiments (González-Pinzón et al., 2013) are well represented by a one-dimensional diffusion model of hyporheic exchange where the effective diffusivity decays exponentially with depth into the streambed. Specifically, statistical moments of the tracer breakthrough curves scale as a function of distance from the injection point in a way that is consistent with the exponential diffusion model but not consistent with other proposed models of hyporheic exchange (Bottacin-Busolin, 2017, 2019).

Hyporheic exchange strongly influences the fate and transport of nutrients, particularly in headwater streams (Boano et al., 2014; Fellows et al., 2006; Hester et al., 2017; Marzadri et al., 2017; Thomas et al., 2001), by regulating their transfer between relatively fast moving water in the bulk stream and pore fluids in the streambed where large residence times and actively growing microbial communities provide an ideal environment for nutrient cycling (Azizian et al., 2015; Boano et al., 2014; Boulton et al., 2010; Zarnetske et al., 2011a). This important topic area has attracted researchers across many different fields, including hydrology, environmental science, engineering, and ecological sciences, to name a few. Because each field brings its own terminology and methodological approaches (Gooseff, 2010), there is a pressing need for unifying conceptual and modeling frameworks that leverage insights across multiple disciplines into a synthetic whole.

In this paper we present one such framework that directly links the one-dimensional diffusion model for hyporheic exchange described above with a key ecological metric of nutrient spiraling called the "uptake velocity." The uptake velocity, which is defined as the ratio of a nutrient's benthic flux and stream concentration, represents a type of standardized mass transfer coefficient for nutrient removal that can be compared across sites (Newbold et al., 1981; Plont et al., 2020; Runkel, 2007; Stream Solute Workshop, 1990; Webster & Patten, 1979) and across nutrients (e.g., nitrate vs. ammonium uptake and denitrification vs. carbon metabolism (O'Brien & Dodds, 2010; Plont et al., 2020; Webster et al., 2003)). We evaluate this new modeling framework in two steps. First, we reanalyze 106 previously published laboratory measurements of hyporheic exchange to evaluate the performance of the one-dimensional diffusion model and the depth-dependence of the effective diffusivity across a wide range of experimental approaches, streambed morphologies, hydraulic conditions, and sediment properties. Simple regression models are prepared for the inferred hyporheic exchange parameters, so that these lab-scale studies can be extrapolated to other experimental and field systems. Second, the regression models are applied to previously published nitrate uptake velocities measured in 72 headwater streams across the United States, collected as part of the Lotic Intersite Nitrogen Experiment (LINX II) (Beaulieu et al., 2011; Hall et al., 2009; Mulholland et al., 2008; Wymore et al., 2019).

2. Modeling Framework for Nutrient Cycling in Streams

In this section we derive a simple resistor-in-series model for the uptake velocity, v_f [LT^{-1}], and explore its asymptotic behavior.

2.1. Resistor-In-Series Representation of the Uptake Velocity

The derivation starts with a conceptual model in which nutrient transfer from the stream to the streambed occurs in three steps (Figures 1a and 1b). In the first step, a nutrient molecule in the bulk stream is vertically transported by stream turbulence through the water column and across a concentration boundary layer located just above the sediment-water interface. This first step can be represented mathematically by a convective mass transfer coefficient, k_m [LT^{-1}] (Step 1 in Figure 1b):

$$J_{bed} = k_m(C_{str} - C_{SWI}) \quad (1)$$

Variables appearing here include the vertical flux of a nutrient from the stream to the streambed, J_{bed} [$ML^{-2}\,T^{-1}$], the nutrient concentration in the bulk stream, C_{str} [ML^{-3}], and the nutrient concentration just above the sediment-water interface, C_{SWI} [ML^{-3}]. A positive flux, $J_{bed} > 0$, denotes a net transfer of nutrients from the bulk stream to the sediment-water interface. The mass transfer coefficient, k_m, represents the velocity with which mass is "squeezed" across the concentration boundary layer by stream turbulence (Grant & Marusic, 2011). According to surface renewal theory, the mass transfer coefficient can be estimated from the stream's shear velocity, u_*, and

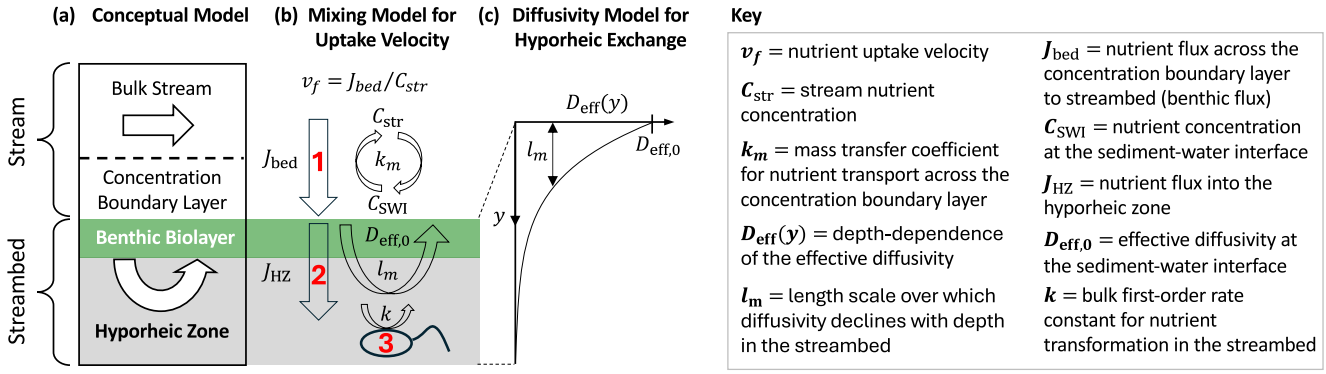

Figure 1. Conceptual and mathematical model for the uptake velocity of nutrients and other reactive contaminants in streams. (a) Conceptual model. (b) Nutrient transport across the concentration boundary layer by stream turbulence (Step 1) is coupled to nutrient transport into the streambed by hyporheic exchange (Step 2) and biotic (or abiotic) reactions in the streambed (Step 3). These three steps are indicated in the figure by bold red numbers. (c) Transport of nutrients into the streambed by hyporheic exchange is modeled by an effective diffusivity that declines exponentially with depth into the sediment (see Equation 3).

Schmidt Number, *Sc* [-], where the latter represents the ratio of molecular diffusion of momentum and mass in the stream (Grant, Azizian, et al., 2018; O'Connor & Hondzo, 2008):

$$k_m = 0.17 u_* Sc^{-2/3} \tag{2a}$$

$$Sc = \frac{\nu}{D_m} \tag{2b}$$

The variables ν [$L^2\ T^{-1}$] and D_m [$L^2\ T^{-1}$] represent the kinematic viscosity of water and the molecular diffusion coefficient of the nutrient, respectively.

As documented by Anlanger et al. (2021), measurements of nutrient uptake by epibenthic biofilms growing in a gravel stream agree closely with predictions from surface renewal theory. Further, these researchers found that both measurements and surface renewal theory predictions of nutrient uptake at the patch scale (O(1 m)) can be extrapolated to nutrient uptake at the stream reach scale (O(1 km)) by spatial averaging.

Once a nutrient molecule reaches the sediment-water interface, in the second step it is transported across the benthic biolayer, which generally includes both autotrophic and heterotrophic microorganisms, and into streambed by myriad hyporheic exchange mechanisms (Step 2 in Figure 1b). In this paper we approximate this second transport step as a one-dimensional diffusion process, with an effective diffusivity that is either constant or decays exponentially with depth. Mathematically this implies that the effective diffusivity can be represented as follows where $D_{eff,0}$ [$L^2\ T^{-1}$] is the effective diffusivity at the sediment-water interface and l_m [L] is the mixing length-scale over which the effective diffusivity decays with depth y into the streambed (Figure 1c):

$$D_{eff}(y) = D_{eff,0} e^{-\frac{y}{l_m}} \tag{3}$$

The effective diffusivity is constant with depth in the limit, $l_m \to \infty$. In the event that hyporheic exchange occurs by bedform pumping, our earlier discussion (Section 1) suggests that the mixing length scale is roughly equal to the bedform wavelength, $l_m \approx \lambda$. A central hypothesis of our paper is that Equation 3 approximates many, though likely not all, hyporheic exchange mechanisms.

In the third step, the nutrient molecule undergoes various transformation reactions as it contacts the benthic biolayer and mixes into the hyporheic zone. The reaction step is represented here by a bulk first-order reaction with rate constant, k [T^{-1}] (Step 3 in Figure 1b).

Given this conceptual model, a steady-state mass balance over a differential slice of pore fluids in the streambed yields the following equation for nutrient flux through the benthic biolayer and hyporheic zone, J_{HZ} [$ML^{-2}\ T^{-1}$], where K_0 and K_1 are modified Bessel functions of the second kind (see Text S1 in Supporting Information S1 for derivation):

$$J_{HZ} = C_{SWI}\sqrt{kD_{\text{eff},0}}F(Da) \tag{4a}$$

$$F(Da) = \frac{K_0(2\sqrt{Da})}{K_1(2\sqrt{Da})} \tag{4b}$$

$$Da = \frac{kl_m^2}{D_{\text{eff},0}} \tag{4c}$$

The dimensionless Damköhler Number, Da, is the ratio of rates for in-bed reaction, k, and in-bed hyporheic zone mixing, $D_{\text{eff},0}/l_m^2$. Equating nutrient fluxes across the concentration boundary layer by stream turbulence, J_{bed}, and into the hyporheic zone by hyporheic exchange and reaction, θJ_{HZ}, solving for the concentration at the sediment-water interface, and substituting the result into Equation 1, we arrive at the following formula for nutrient flux into the streambed:

$$J_{bed} = k_m C_{str}\left(1 - \frac{1}{1 + \frac{\theta\sqrt{kD_{\text{eff},0}}}{k_m}F(Da)}\right) \tag{5}$$

The streambed porosity, θ, was included in the flux matching condition, $J_{bed} = \theta J_{HZ}$, to ensure mass conservation across the sediment-water interface (Grant et al., 2012). From this last result we can also derive a solution for the uptake velocity which, by definition, equals the benthic flux of the nutrient into the stream bed, J_{bed}, divided by the nutrient concentration in the bulk stream, C_{str}:

$$v_f = \frac{J_{bed}}{C_{str}} = k_m\left(1 - \frac{1}{1 + \frac{\theta\sqrt{kD_{\text{eff},0}}}{k_m}F(Da)}\right) \tag{6}$$

Inverting Equation 6 we arrive at a remarkably simple expression for the total mass transfer resistance for nutrient uptake in the hyporheic zone, R_T [TL^{-1}] (Figure 2a):

$$\frac{1}{v_f} = R_T = R_1 + R_2 \tag{7a}$$

$$R_1 = \frac{1}{k_m} \tag{7b}$$

$$R_2 = \frac{1}{\theta\sqrt{kD_{\text{eff},0}}F(Da)} \tag{7c}$$

The total mass transfer resistance, R_T, is a measure of how difficult it is to remove a nutrient molecule from the stream by hyporheic exchange and reaction; that is, the larger the resistance the more difficult nutrient removal becomes. Because a nutrient molecule must first traverse the concentration boundary layer before entering the streambed, the in-stream and in-bed mass transfer resistances act in series (Figure 2a); that is, R_1 and R_2 are additive in Equation 7a. One implication is that when $R_1 \gg R_2$, mass transport across the concentration boundary layer becomes a "bottleneck" for nutrient uptake by the streambed. Put another way, convective mass transport across the concentration boundary layer imposes an upper limit on the uptake velocity (Grant, Azizian, et al., 2018).

The above formulae are premised on the idea that the diffusivity decays exponentially with depth into the streambed. If the diffusivity is constant with depth (i.e., $l_m \to \infty$), all of the above results remain unchanged, except the function $F(Da)$ is equal to unity, $F_{l_m\to\infty}(Da) = 1$. The asymptotic behavior of this resistor-in-series model for the uptake velocity is discussed next.

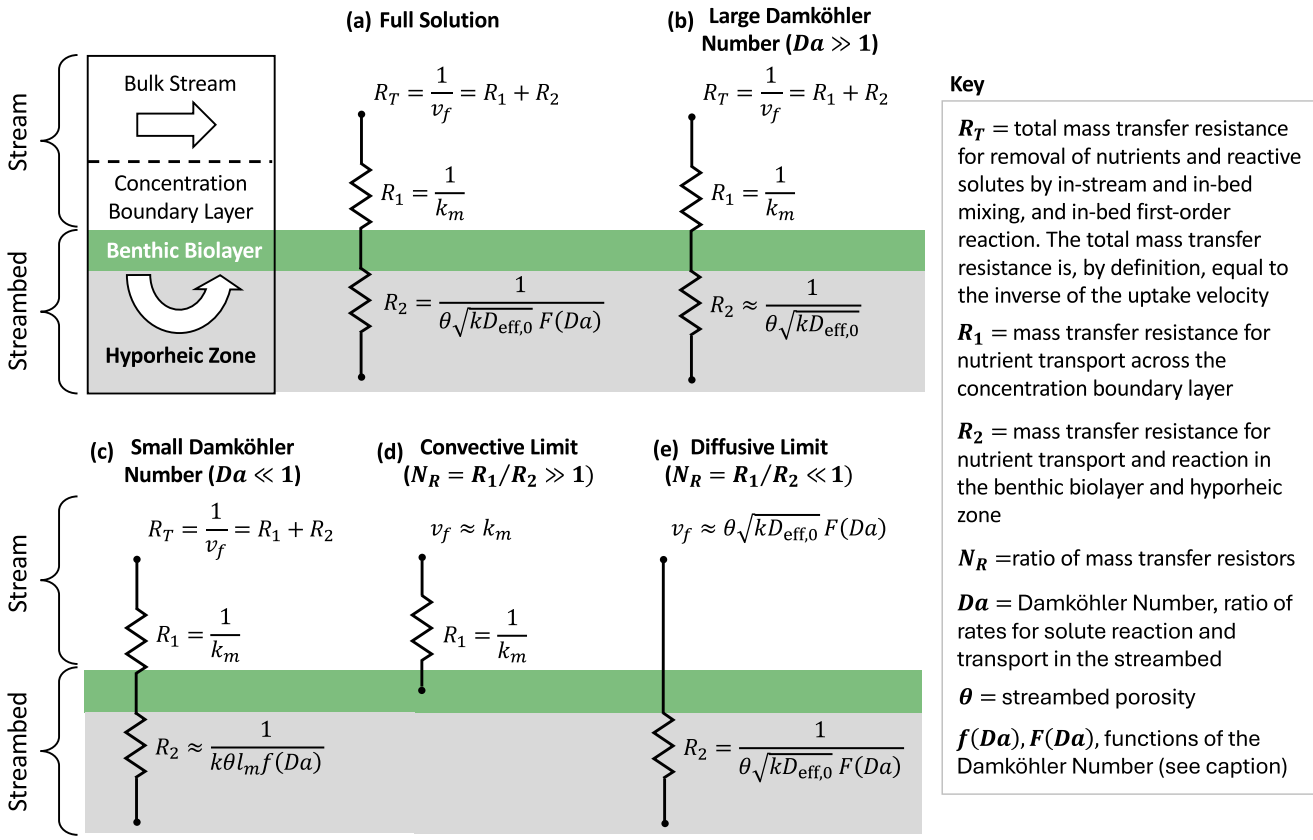

Figure 2. A resistor-in-series model for the uptake velocity, v_f, of nutrients and other reactive contaminants in streams. (a) Under steady-state conditions the inverse of the uptake velocity is equal to the total mass transfer resistance, $1/v_f = R_T$. The total resistance, in turn, is equal to the sum of two mass transfer resistors in series, one accounting for in-stream mixing across the concentration boundary layer (R_1) and another accounting for in-bed mixing and first-order reaction (R_2): $R_T = R_1 + R_2$. Panels (b–e) asymptotic behavior of the resistor-in-series model based on the magnitudes of the Damköhler Number, Da, and the resistor ratio, $N_R = R_1/R_2$. The functions appearing in the definition of R_2 are defined as follows: $F(Da) = K_0(2\sqrt{Da})/K_1(2\sqrt{Da})$ and $f(Da) = -2\gamma - lnDa$, where K_0 and K_1 are Bessel functions of the second kind and γ is Euler's Number (see main text). Variables not defined here are defined in Figure 1.

2.2. Asymptotic Behavior of Resistor-In-Series Model

The expressions derived above for nutrient uptake velocity—or its inverse the total mass transfer resistance—simplify when certain variables become either large or small. For example, we note that the function, $F(Da)$, ranges from 0 to 1, where the upper and lower-limits correspond to $Da \to 0$ and $\to \infty$, respectively. Therefore, when the Damköhler Number is large (i.e., rate of reaction in the streambed is fast relative to the rate of hyporheic exchange), the second mass transfer resistance simplifies as follows, $R_2 = 1/\theta\sqrt{kD_{\mathrm{eff},0}}$ ($Da \gg 1$, Figure 2b). Note that this simplification also applies when the effective diffusivity is constant with depth (i.e., $l_m \to \infty$, see last section). Further, if the resistance for mass transfer across the concentration boundary layer is relatively small (i.e., $R_2 \gg R_1$) then the uptake velocity becomes, $v_f \approx \theta\sqrt{kD_{\mathrm{eff},0}}$ when $Da \gg 1$.

In the opposite limit, when the Damköhler Number is small, $0 < Da \ll 1$, the rate of reaction in the streambed is slow relative to the rate of hyporheic exchange. The asymptotic behavior of $F(Da)$ in this limit can be found by performing a first-order Taylor Series expansion of Equation 4b around $Da = 0$: $F(Da) \approx \sqrt{Da} f(Da)$, where $f(Da) = -\ln Da - 2\gamma$ and $\gamma \approx 0.5772$ is Euler's constant. Thus, in this small Damköhler Number limit, the second mass transfer resistance becomes, $R_2 \approx 1/k\theta l_m f(Da)$ (Figure 2c). Further, if the resistance for mass transfer across the concentration boundary layer is relatively small, $R_2 \gg R_1$, then the uptake velocity becomes, $v_f \approx k\theta l_m f(Da)$ when $0 < Da \ll 1$. Under these conditions, the uptake velocity depends only on the first-order reaction rate constant k and the volume (per unit bed area) of interstitial fluids in the hyporheic zone, $\theta l_m f(Da)$; in effect, the hyporheic zone is a well-mixed reactor. The effective depth of this well-mixed reactor, $l_m f(Da)$, depends on l_m and the Damköhler Number through the functional dependence, $f(Da)$. All else being

equal, the effective depth of the well-mixed reactor increases with decreasing Da. Interestingly, the commonly used transient storage model for solute transport in streams assumes that the hyporheic zone is a well-mixed reactor (Knapp & Kelleher, 2020). Thus, the transient storage model can be viewed as a special case of our more general theory.

The relative importance of in-stream mixing versus in-bed mixing and first-order reaction is defined by the ratio of the two mass transfer resistances:

$$N_R = \frac{R_1}{R_2} = \frac{\sqrt{Da}F(Da)}{Bi} \tag{8a}$$

$$Bi = \frac{k_m l_m}{\theta D_{\text{eff},0}} \tag{8b}$$

The Biot Number, Bi, describes the relative rates of convective mass transport across the concentration boundary layer and mixing by hyporheic exchange in the streambed (Grant, Gomez-Velez, & Ghisalberti, 2018). In-stream mixing controls the uptake velocity, $v_f \approx k_m$, when $N_R \gg 1$ or, equivalently, when $Da \gg 1$ and $Bi \ll 1$ (Figure 2d). In-bed mixing and first-order reaction control the uptake velocity, $v_f \approx \theta\sqrt{kD_{\text{eff},0}}F(Da)$, when $N_R \ll 1$ or, equivalently, when $Da \ll 1$ and $Bi \gg 1$ (Figure 2e).

2.3. Experimental and Field Testing the Resistor-In-Series Model

We evaluated the resistor-in-series model in two steps. First, we tested the exponential diffusion model for hyporheic exchange (Equation 3 and Figure 1c) against laboratory measurements of hyporheic exchange collected over a wide range of exchange mechanisms, hydraulic conditions, sediment properties, and experimental designs (Sections 3.1 and 4.1). A key outcome of this first step is a validation of Equation 3 and a set of regression relationships for the diffusivity model's two key parameters ($D_{\text{eff},0}$ and l_m) that can be applied to other laboratory and field systems. Second, we applied these regression relationships to nitrate uptake velocities measured in headwater streams draining urban, agricultural and reference landscapes throughout the United States (Sections 3.2 and 4.2). Key outcomes of this second step include estimates of the first-order rate constant for nitrate removal in the streambed by assimilation and denitrification (k in Figure 1b), regression relationships for these rate constants, and new insights into how land-use, stream physics, and biological processes collectively influence in-stream and in-bed mixing and nitrate uptake in headwater streams.

3. Methods

3.1. Testing the Diffusive Model of Hyporheic Exchange

There is ample evidence from laboratory and field studies that the mass transfer of solutes across the concentration boundary layer above a streambed (Step 1 in Figure 1b) is well-described by surface renewal theory (see Equations 1 and 2a and discussion thereof) (Grant & Marusic, 2011; O'Connor & Hondzo, 2008; O'Connor et al., 2009). What is less clear is whether the exponential diffusivity model adequately represents hyporheic exchange (Step 2 in Figure 1b). This knowledge gap was addressed as follows.

3.1.1. Previously Published Laboratory Data

The exponential diffusivity model (Equation 3) was tested on 106 previously published laboratory flume and stirred tank measurements of hyporheic exchange. These experiments all used a conservative solute to measure hyporheic exchange over a wide range of hydrodynamic conditions and sediment bed properties and morphologies, including flat beds (66 experiments), ripples and dunes (28 experiments), and alternate bars (12 experiments) (Chandler et al., 2016; Elliott & Brooks, 1997b; Eylers, 1994; Lai et al., 1994; Packman & MacKay, 2003; Packman et al., 2000, 2004; Rehg et al., 2005; Richardson & Parr, 1988; Tonina & Buffington, 2007). These experiments also differed relative to (a) the nature of the laboratory set-up used to measure hyporheic exchange, including recirculating flumes (46 experiments), stirred tanks (23 experiments), and once-pass through flumes (37 experiments); and (b) the initial condition adopted, including a conservative dye initially placed in the water column (46 experiments) or a conservative dye initially placed in the pore fluids of the streambed (60 experiments). In recirculating flume and stirred tank experiments, which are closed systems, hyporheic exchange is

measured by the rate at which solute concentrations in the overlying water column and sediment pore fluids approach a well-mixed equilibrium state; that is, faster hyporheic exchange manifests as a faster approach to equilibrium. In the once-pass through flume experiments, which are open systems, clean (solute-free) water is continuously run over the top of a streambed that is initially saturated with solute. Hyporheic exchange is measured by the rate at which solute mass discharged from the flume drops to zero; that is, faster hyporheic exchange manifests as a faster "wash-out" of solute from the streambed. Key attributes of each experiment are summarized in Table S1 in Supporting Information S1.

3.1.2. Analytical Solutions to the Exponential Diffusivity Model

Different analytical solutions to the diffusivity model were applied to the above experimental data, depending on the presumed depth profile of the effective diffusivity (the effective diffusivity is constant (C-profile) or declines exponentially with depth (E-profile)), whether the experiment was conducted in a closed (recirculating flume and stirred tank) or open (once pass-through flume) system, and the nature of the sediment bed's lower boundary condition (finite or infinite in extent). Details are presented in Text S1–S4 in Supporting Information S1.

3.1.3. Diffusivity Model Performance and Parameter Inference

Values for the effective diffusivity at the sediment-water interface ($D_{\text{eff},0}$, both C- and E-profiles) and the mixing length-scale (l_m, E-profile only) were inferred by minimizing the root mean squared error (RMSE) between observed and model-predicted concentrations in the water column (closed systems, 69 studies) or instantaneous mass discharge of solute out of the flume (open systems, 37 studies). Model performance was evaluated based on RMSE, corrected Akaike Information Criterion (AICc, which identifies the most parsimonious model based on a balance between model fit and the number of model parameters (Akaike, 1974; Brewer et al., 2016)), and Nash-Sutcliffe Efficiency (NSE, which ranges from 0 to 1, where the lower limit indicates that the model represents the data no better than the mean and the upper limit indicates a perfect representation of the data (Weglarczyk, 1998)). All calculations were carried out in Wolfram Mathematica (v 14).

3.1.4. Regression Relationships for $D_{\text{eff},0}$ and l_m

Because the hyporheic exchange experiments included in this study were all conducted under well-characterized and well-controlled conditions, inferred values of $D_{\text{eff},0}$ and l_m can be regressed against measured physical, hydraulic, and sediment properties with the goal of deriving simple formulae for these diffusivity parameters that can be applied to other experimental or field systems.

To this end, we conducted a set of multiple linear regression (MLR) studies, adopting $D_{\text{eff},0}$ and l_m as the two dependent variables and the following reported features of each laboratory experiment as potential explanatory variables: (a) water column height h_w [L]; (b) shear velocity u_* [LT^{-1}]; (c) kinematic viscosity of water ν [$\text{L}^2\ \text{T}^{-1}$]; (d) molecular diffusion coefficient of the tracer D_m [$\text{L}^2\ \text{T}^{-1}$]; (e) sediment porosity θ [-], depth d_b [L], permeability K [L^2], median grain size d_{50} [L], and morphology (flat bed, bedforms, or alternate bars); (f) bedform height h_b [L] and wave number $w_n = 2\pi/\lambda$ [L^{-1}] where λ [L] is the wavelength of the bedform; and (g) bed roughness $k_s = 3d_{90} + 1.1h_b\left(1 - e^{-25h_b/\lambda}\right)$ [L] (O'Connor & Harvey, 2008) where d_{90} [L] is the 90th percentile sediment grain size. For flat beds the height and wavelength variables become, $h_b \to 0$ and $\lambda \to \infty$, respectively. The depth-averaged stream velocity was not included in this list because it has no meaning in the context of stirred tank experiments.

Sediment bed morphology was treated as a binary variable where, for example, $F(0, 1) = 1$ or 0 indicates the sediment bed was either flat or not, respectively. Only two binary bed morphology variables were included in the MLR (flat bed $F(0, 1)$ and bedform $B(0, 1)$) because the third is implied by the value of the other two (Alkharusi, 2012); for example, if the sediment bed is not flat, $F(0, 1) = 0$, and does not have bedforms, $B(0, 1) = 0$, it must have alternate bars. Because many of the continuous independent variables varied over multiple orders of magnitude, and to improve the normality of residuals, we assumed a power-law relationship between dependent and continuous independent variables (Grant et al., 2012). An exponential functional relationship was assumed for the binary variables $F(0, 1)$ and $B(0, 1)$, to avoid singularities in the regression model when either binary variable equals zero. Given these preliminaries, the log-transformed regression equations for $D_{\text{eff},0}$ and l_m take on the following linear form (C. Y. Chen et al., 2024; Grant et al., 2012):

$$\ln D_{\text{eff},0} = A_1 + B_1 \ln h_w + C_1 \ln u_* + D_1 \ln d_b + E_1 \ln K + F_1 \ln d_g + G_1 \ln k_s + H_1 \ln \nu + I_1 \ln D_m + J_1 \ln h_b + K_1 w_n + L_1 \ln \theta + M_1 F(0, 1) + N_1 B(0, 1) \quad (9a)$$

$$\ln l_m = A_2 + B_2 \ln h_w + C_2 \ln u_* + D_2 \ln d_b + E_2 \ln K + F_2 \ln d_g + G_2 \ln k_s + H_2 \ln \nu + I_2 \ln D_m + J_2 \ln h_b + K_2 w_n + L_2 \ln \theta + M_2 F(0, 1) + N_2 B(0, 1) \quad (9b)$$

The factors $A_1,\ldots,N_1$ and $A_2,\ldots,N_2$ are the regression coefficients to be determined. Prior to performing the MLR, the Variance Inflation Factor (VIF) of all potential explanatory variables was calculated; explanatory variables with VIF >5 (indicating strong covariance with other explanatory variables) were removed (Ott & Longnecker, 2004). The dependent variables, $\ln D_{\text{eff},0}$ and $\ln l_m$, were then regressed against all possible combinations of the potential explanatory variables appearing on the right hand side of Equations 9a and 9b (glmulti package in R (Calcagno & Mazancourt, 2010)). This process generates a population of candidate regression models, some with only a single explanatory variable, some with different combinations of two explanatory variables, and so on. From this list we selected final regression models for $D_{\text{eff},0}$ and l_m in three steps. First, we removed any candidate models for which one or more regression coefficients were not significantly different than zero at p-value ≤ 0.01. Second, the remaining candidate models were ranked by AICc, where the model with the lowest AICc is the most parsimonious (Brewer et al., 2016). Finally, candidate models with the lowest AICc were selected. Because AICc penalizes models that contain explanatory variables that confer only marginal improvements to overall model fit, the final top-ranked models for $D_{\text{eff},0}$ and l_m are likely to have fewer variables than those listed on the right hand side of Equations 9a and 9b, respectively.

3.2. Field Application of the Resistor-In-Series Model

3.2.1. LINX II Measurements of Nitrate Uptake Velocity

The resistor-in-series model (Equation 6) was applied to nitrate uptake velocities measured in 72 headwater streams during LINX II, which occurred over 5 years from 2001 to 2006 (Beaulieu et al., 2011; Hall et al., 2009; Mulholland et al., 2008, 2009). At each LINX II site ^{15}N-labeled nitrate was continuously injected into the stream and simultaneously measured a fixed distance downstream. From these data, LINX II researchers calculated the removal of nitrate by both assimilation and denitrification ("total nitrate uptake velocity," $v_{\text{f,tot}}$) and denitrification alone ("denitrification uptake velocity," $v_{\text{f,den}}$). Application of the resistor-in-series model to the LINX II data set required site-specific estimates for in-stream and in-bed transport parameters as follows.

3.2.2. Estimating Transport Parameters at the LINX II Sites

The three transport parameters (k_m, $D_{\text{eff},0}$, and l_m, see Figure 1b) were estimated for each LINX II site from regression formulae (presented later in Section 4.1.3) using site-specific values of the shear velocity, stream slope, stream water depth, and temperature-dependent values for the molecular diffusion coefficient of nitrate in water and kinematic viscosity (see Table S1 in the Supporting Information of Grant, Azizian, et al. (2018)). Following Marzadri et al. (2014), we set the streambed porosity across all LINX II sites equal to $\theta = 0.32$ and used the following empirical formula to estimate hydraulic conductivity, K_h, from site-specific measurements of median grain diameter, d_{50}: $K_h = 16.88 + 10.6 d_{50}$ (Salarashayeri & Siosemarde, 2012), where K_h is in units of meters per day and d_{50} is in units of mm. Hydraulic conductivity was then converted to sediment permeability as follows, $K = K_h \nu / g$, where ν is the kinematic viscosity of water and $g = 9.81$ m^2 s^{-1} is the gravitational acceleration constant.

3.2.3. Regression Relationships for the First-Order Rate Constant

As described in Section 4.2.2, application of the resistor-in-series model to the LINX II data set allowed us to infer, for each site, first-order rate constants for in-bed removal of nitrate by assimilation and denitrification, k_{tot}, and denitrification alone, k_{den}. A set of MLR studies were then carried out, in which inferred values of k_{tot} and k_{den} were taken as the dependent variables and the following measured properties at each LINX II site were adopted as potential explanatory variables: (a) median grain diameter d_{50} [L]; (b) stream nitrate concentration $\left[NO_3^-\right]$ [M L^{-3}]; (c) gross primary production (GPP) and ecosystem respiration (ER) [M L^{-2} T^{-1}]; (d) the ratio between GPP and ER which indicates whether autotrophy (GPP/ER >1) or heterotrophy (GPP/ER <1) dominates stream metabolism

(Plont et al., 2020); (e) stream temperature T (Celsius); and (f) binary variables for land-use type, including agriculture AGR(0, 1) and urban URB(0, 1) land-use where, for example, AGR(0, 1) = 1 or 0 indicates streams that drain agricultural areas or not. Reference land-use is implied by the values AGR(0, 1) = 0 and URB(0, 1) = 0 (see Section 3.1.4 for discussion of implicit binary variables). Adopting power-law and exponential functional relationships for the continuous and binary variables, respectively, the log-transformed regression equations for k_{tot} and k_{den} take on the following linear form:

$$\ln k_{tot} = A_3 + B_3 \ln d_{50} + C_3 \ln\left[NO_3^-\right] + D_3 \ln \mathrm{GPP} + E_3 \ln \mathrm{ER} + F_3 \ln \frac{GPP}{ER} + G_3 \ln \mathrm{T} + H_3 \mathrm{AGR}(0,\,1) + I_3 \mathrm{URB}(0,\,1) \tag{10a}$$

$$\ln k_{den} = A_4 + B_4 \ln d_{50} + C_4 \ln\left[NO_3^-\right] + D_4 \ln \mathrm{GPP} + E_4 \ln \mathrm{ER} + F_4 \ln \frac{GPP}{ER} + G_4 \ln \mathrm{T} + H_4 \mathrm{AGR}(0,\,1) + I_4 \mathrm{URB}(0,\,1) \tag{10b}$$

Here, the factors $A_3,\ldots,I_3$ and $A_4,\ldots,I_4$ are regression coefficients to be determined. Any potential explanatory variables with VIF >5 were removed prior to performing the MLR. As described in Section 3.1.4, a population of regression models were generated for all possible combinations of the potential explanatory variables (glmulti package in R (Calcagno & Mazancourt, 2010)). Regression models were removed if one or more explanatory variables were not significant at $p < 0.01$. The remaining models were then ranked by AICc and the most parsimonious models for k_{tot} and k_{den} were selected for further consideration.

4. Results and Discussion

4.1. Laboratory Testing the Diffusivity Model of Hyporheic Exchange

To test Equation 3 we: (a) determined which diffusivity depth profile (C-profile or E-profile) best represents laboratory measurements of hyporheic exchange (Section 4.1.1); and (b) evaluated how the inferred parameter values differ depending on whether the model assumes the sediment bed is finite or infinite in extent (Section 4.1.2). We then developed simple regression formulae for the diffusivity model's inferred parameters that can be applied to other laboratory and field systems (Section 4.1.3).

4.1.1. Diffusivity Depth Profile

The RMSE between measured and model-predicted water column solute concentrations (closed systems) or solute fluxes (open systems) were computed for all 106 laboratory hyporheic exchange experiments included in this study. This RMSE calculation was carried out twice, once using the analytical solution for the constant diffusivity profile (C-profile, RMSE_C), and again using the analytical solution for an exponentially declining diffusivity profile (E-profile, RMSE_E). Both of these analytical solutions assumed that the sediment bed is finite in extent; that is, a no-flux boundary condition is imposed at $y = d_b$, where d_b equals the reported depth of the sediment bed. The normalized difference between these two RMSE values, $\Delta\mathrm{RMSE} = (\mathrm{RMSE}_E - \mathrm{RMSE}_C)/\mathrm{RMSE}_E$, is a measure of whether the C-profile model ($\Delta\mathrm{RMSE} > 0$) or E-profile model ($\Delta\mathrm{RMSE} < 0$) better represents the concentrations or fluxes measured in a particular experiment. The E-profile model had lower error in 89 of the 106 experiments (i.e., $\Delta\mathrm{RMSE} < 0$, blue bars on left side of Figure 3a). Further, across all experiments the E-profile is a reasonable representation of the measured normalized concentration or flux based on both the model's RMSE (<2.4% error) and NSE (95% of experiments had a NSE > 0.88).

Because the E-profile model has one more parameter than the C-profile model, the former's superior performance could be an artifact of overfitting. To investigate this possibility, we repeated the above analysis after replacing RMSE with AICc, which penalizes models with more parameters: $\Delta\mathrm{AICc} = (\mathrm{AICc}_E - \mathrm{AICc}_C)/\mathrm{AICc}_E$. Values of $\Delta\mathrm{AICc} < 0$ or >0 indicate a higher ranking for the E-profile model or C-profile model, respectively. Based on AICc, the E-profile model still outperforms the C-profile model in 83 of the 106 experiments (blue bars on right side of Figure 3a). Further, an experimental artifact is implicated for most (18 of 23) of the experiments for which the C-profile is superior. Namely, in these experiments the sediment bed depth was less than 30% of the inferred mixing length-scale (i.e., $d_b/l_m < 0.3$), implying that hyporheic exchange flows likely "felt the bottom" of the

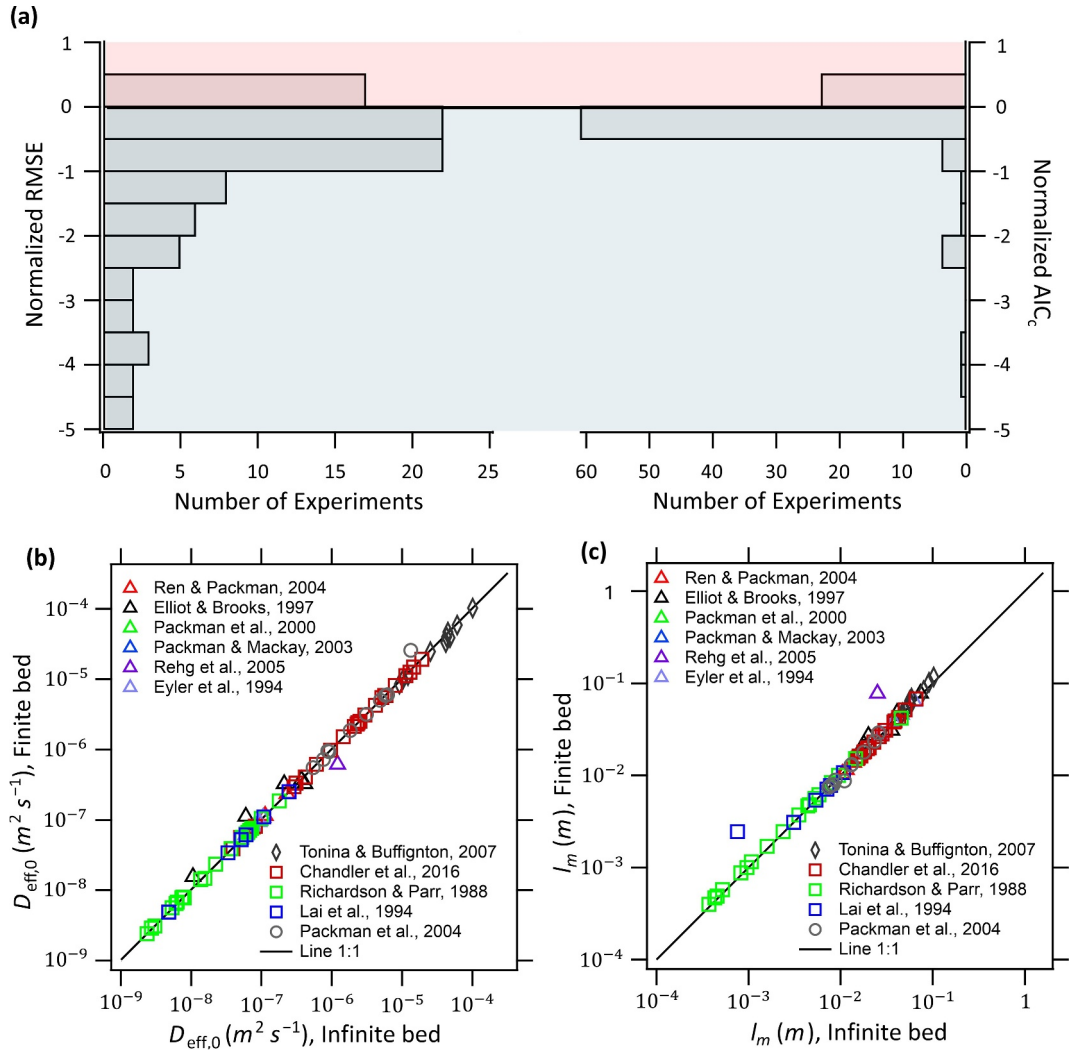

Figure 3. Evaluation of the diffusivity model for hyporheic exchange based on 106 previously published laboratory experiments. (a) The model's diffusivity depth-profile (C- or E-profiles) was evaluated using either normalized root mean squared error or normalized AICc as the model metric. Red or blue regions indicate experiments for which the C- or E-profiles, respectively, are superior. (b and c) The influence of the model's bottom boundary condition (finite or infinite) on inferred values of the E-profile's effective diffusivity at the sediment-water interface (panel b) and mixing depth (panel c). The one-to-one line indicates a perfect correspondence.

sediment bed in these cases. In summary, the E-profile (i.e., Equation 3 with a finite value of l_m) is a robust representation of hyporheic exchange in both closed and open systems, across various experimental designs (recirculating flumes, stirred tanks, once pass-through flumes) and for a wide range of sediment bed morphologies, sediment properties, and hydraulic conditions.

4.1.2. Influence of the Bottom Boundary

Next we investigated how the assumed bottom boundary condition in the model (either finite or infinite in extent) influences inferred values of the E-Profile's two parameters, $D_{eff,0}$ and l_m. Across the 83 experiments for which the E-profile was superior (i.e., $\Delta AICc < 0$), estimates for these two parameters vary over 5 and 2.5 orders of magnitude, respectively, from $D_{eff,0} \approx 10^{-9}$ to 10^{-4} m^2 s^{-1} and from $l_m \approx 10^{-3.5}$ to 0.1 m (Figures 3b and 3c). For these 83 experiments, values of $D_{eff,0}$ and l_m inferred from the finite and infinite bed models are the same within error (i.e., they plot close to the one-to-one line in Figures 3b and 3c). As long as the inequality, $d_b/l_m > 0.3$, is satisfied, the finite depth of the hyporheic zone does not need to be explicitly represented. Note that our resistor-in-series model for the uptake velocity (Equation 6) assumes that the streambed is infinitely deep.

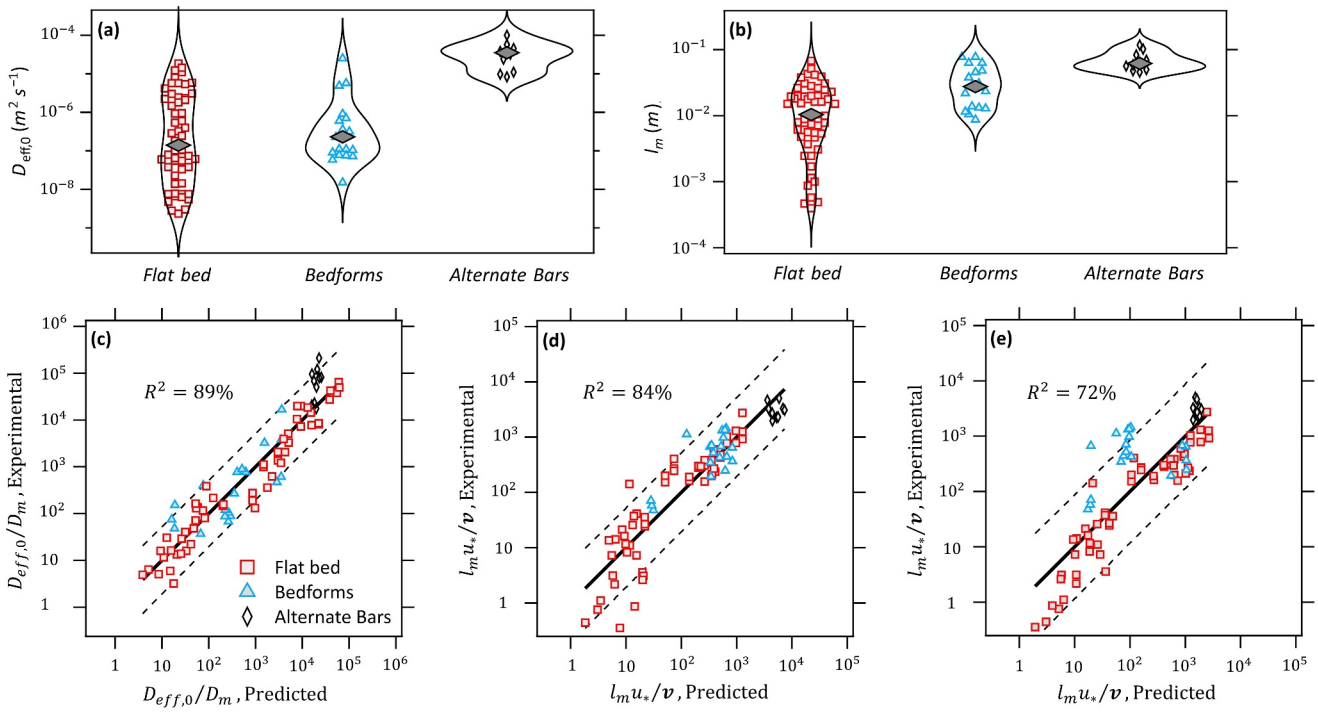

Figure 4. The influence of sediment bed morphology (flat bed, bedforms, or alternate bars) on inferred values of (a) effective diffusivity at the sediment-water interface and (b) mixing depth from laboratory measurements of hyporheic exchange. The performance of multiple linear regression models for (c) effective diffusivity at the sediment-water interface (Equation 12a), (d) mixing depth (Equation 12b), and (e) mixing depth without the inclusion of the bed roughness Reynolds Number (Equation 13). Solid lines represent a perfect correspondence between experimental and regression model-predicted values. Dashed lines represent the 90% prediction interval for each regression.

Thus, in cases where the depth of the hyporheic zone is less than 30% of the mixing length, l_m, the resistor-in-series model may need to be modified to explicitly account for the bottom boundary.

4.1.3. Regression Relationships for $D_{\text{eff},0}$ and l_m

In preparing regression equations for the E-profile's two parameters, $D_{\text{eff},0}$ and l_m, we included only laboratory experiments for which the inequality $\Delta\text{AICc} < 0$ was satisfied (see last section). That left a total of 83 experiments for inclusion in the MLR study, including 54 experiments with flat beds, 19 with bedforms (ripples or dunes), and 10 with alternate bars. Values of $D_{\text{eff},0}$ and l_m inferred from fitting Equation 3 to these 83 experiments varied by sediment bed morphology (Figures 4a and 4b), with median values increasing in order: flat bed ($10^{-6.9}$ m^2s^{-1} and 1 cm) < bedforms ($10^{-6.6}$ m^2s^{-1} and 3 cm) < alternate bars ($10^{-4.5}$ m^2s^{-1} and 6 cm). Mixing intensity at the sediment-water interface and the depth to which that mixing penetrates both depend on bed morphology.

To identify other variables that influence in-bed mixing beyond bed morphology, we conducted two rounds of MLR. In the first round we created regression models for $\ln D_{\text{eff},0}$ and $\ln l_m$, excluding any experiments for which the inequality, $d_b/l_m > 0.3$, was not satisfied. Due to high collinearity with other variables (VIF > 5), four independent variables—the binary variable for bedforms $B(0, 1)$ and continuous variables for bedform height h_b, bedform wave number w_n, and sediment porosity θ—were excluded from the MLR analysis. Regression models constructed from all combinations of the remaining variables were ranked by AICc, resulting in the following top-models for the effective diffusivity at the sediment-water interface and mixing depth, expressed here in their exponentiated form (compare with Equations 9a and 9b):

$$D_{\text{eff},0} = 10^{-4.76\pm2.02} k_s^{0.36\pm0.15} u_*^{1.37\pm0.19} K^{0.63\pm0.06} d_b^{-0.48\pm0.21} D_m^{-0.76\pm0.21}, \quad R^2 = 0.89 \tag{11a}$$

$$l_m = 10^{-27.53\pm7.09} k_s^{0.35\pm0.11} u_*^{0.43\pm0.14} \nu^{-3.74\pm1.08} D_m^{-0.52\pm0.17}, \quad R^2 = 0.69 \tag{11b}$$

Given the apparent influence of bed morphology on $D_{\text{eff},0}$ and l_m (see Figures 4a and 4b), it is surprising that the binary variables B(0, 1) and F(0, 1) do not appear in these regressions. As noted earlier, the binary variable for bedforms, B(0, 1), was removed from the MLR due to high colinearity with other independent variables. Further, while some top models included the binary variable for flat beds, F(0, 1), the prefactor for this variable was not significantly different than zero at $p < 0.01$. Finally, because both B(0, 1) and F(0, 1) are not included in the top ranked models, the implicit binary variable for alternate bars is also not included; recall, alternate bars correspond to the case, B(0, 1) = F(0, 1) = 0 (see Methods). Thus, in the context of these regressions, it appears that bed morphology influences in-bed mixing indirectly, rather than directly, by changing bed roughness (k_s) and shear stress (or friction) at the bed (u_*).

In the second round of MLR we derived non-dimensional forms of these two regression equations, with the goal of identifying the fundamental dimensionless numbers that serve as master variables for in-bed mixing by hyporheic exchange. The Buckingham Π Theorem (Buckingham, 1914) suggests that Equation 11a can be recast in terms of five dimensionless numbers, provided that kinematic viscosity, ν, is included in the list of original variables. We adopted a normalized form of the effective diffusivity at the sediment-water interface ($\frac{D_{\text{eff},0}}{D_m}$) as the dependent variable and the following non-dimensionless numbers as potential explanatory variables: (a) bed Reynolds Number (Re_b, representing the ratio of the bed depth and the inner length-scale of the stream's turbulent velocity boundary layer, ν/u_*); (b) the permeability Reynolds Number (Re_K, representing the ratio of the permeability length-scale $\sqrt{K}$ and ν/u_*); (c) the roughness Reynolds Number (Re_*, representing the ratio of the bed roughness length-scale k_s [L] and ν/u_*); and (d) the Schmidt Number ($Sc = \nu/D_m$), representing the ratio of molecular diffusion of momentum and mass through the pore fluids. Likewise, the Buckingham Π Theorem indicates that Equation 11b can be recast in terms of three dimensionless numbers. We adopted a normalized mixing depth ($\frac{l_m u_*}{\nu}$) as the dependent variable and the roughness Reynolds Number Re_* and Schmidt Number Sc as potential explanatory variables. Repeating the MLR analysis with this set of non-dimensional numbers yields the following dimensionless forms of Equations 11a and 11b (Figures 4c and 4d):

$$\frac{D_{\text{eff},0}}{D_m} = 10^{-1.56\pm0.55}\, Re_K^{\,1.34\pm0.05}\, S_c^{\,1.56\pm0.17}, \quad R^2 = 0.89 \tag{12a}$$

$$\frac{l_m u_*}{\nu} = 10^{-2.57\pm0.59}\, Re_*^{\,0.93\pm0.05}\, S_c^{\,0.87\pm0.17}, \quad R^2 = 0.84 \tag{12b}$$

$$Re_K = \frac{u_*\sqrt{K}}{\nu} \tag{12c}$$

$$Re_* = \frac{u_* k_s}{\nu} \tag{12d}$$

Comparing Equations 11a and 12a we note that bed depth d_b and bed roughness k_s appear in the former but not in the latter (i.e., the bed and roughness Reynolds Numbers do not appear on the right hand side of Equation 12a). The bed Reynolds Number was removed due to high collinearity with other variables (VIF = 10). All MLR models containing the roughness Reynolds Number were excluded because the regression coefficient for this dimensionless number was not significantly different than zero at $p < 0.01$. Also note that the coefficient of determination for the mixing depth is higher in its dimensionless form ($R^2 = 0.69$ and 0.84 for Equations 11 and 12b, respectively). This is because the shear velocity appears on both the left and right side of Equation 12b and thus the coefficient of determination is artificially elevated in this case.

The inferred power-law dependence of the effective diffusivity on the permeability Reynolds Number, $D_{\text{eff},0} \propto Re_K^b$ with $b = 1.34$, is consistent with previously published multi-physics model simulations and laboratory measurements of hyporheic exchange across flat beds and bedforms for which with the power-law exponent ranges from $b = 1$ to 2.5 (C. Y. Chen et al., 2024; Grant, Gomez-Velez, et al., 2020; Grant, Monofy, et al., 2020; Voermans et al., 2018). Furthermore, the power-law dependence of the mixing depth l_m on the roughness Reynolds Number, $l_m \propto Re_*^{0.93}$, is similar to the scaling relationship proposed by C. Y. Chen et al. (2024) for the mixing depth associated with turbulent flow over a flat porous bed, $\delta \propto Re_*^{1.01}$. The latter was

estimated from numerical simulations of turbulent flow over a porous bed, where the length-scale δ is referenced relative to the inflection point of the mean velocity profile near the bed (C. Y. Chen et al., 2024).

One potential concern with the regression formulae developed above for l_m (Equations 11 and 12b) is that they depend on the bed roughness k_s or its dimensionless form, the roughness Reynolds Number, Re_*. This variable requires information on bedform height and wavelength—information that may not be available for many streams. We therefore performed one final MLR in which the dimensionless form of l_m was regressed against Re_k and S_c alone. The result (Equation 13, Figure 4e) explains slightly less variance but is likely to be more useful in practice, as demonstrated later in the context of the LINX II data set.

$$\frac{l_m u^*}{\nu} = 10^{1.22\pm0.73}\ Re_K^{\ 1.02\pm0.07}\ S_c^{\ 0.44\pm0.2},\ R^2 = 0.72 \tag{13}$$

In summary, simple regression formulae (Equations 12a and 13) were derived for the exponential model's two key parameters—effective diffusivity at the sediment-water interface and mixing depth—based solely on the stream's permeability Reynolds Number Re_K and Schmidt Number Sc. These two parameter can be readily estimated for a particular stream from the median grain size of the streambed and the stream's depth, slope, and temperature.

4.2. Field Application of the Resistor-In-Series Model

Here we demonstrate that the above regression formulae and the resistor-in-series model for the uptake velocity can be combined to yield new insights into the physical and biological controls on nutrient removal in the hyporheic zone of headwater streams. This analysis was implemented in four steps. First, we estimated values of k_m, $D_{\text{eff},0}$ and l_m for each LINX II site, and then evaluated how these transport parameters vary across streams draining agricultural, urban, and reference land-use types (Section 4.2.1). Using the resistor-in-series model, we then inferred from the measured uptake velocities first-order rate constants for in-bed removal of nitrate by assimilation and denitrification, k_{tot} and denitrification alone, k_{den} (Section 4.2.2) and the corresponding reaction timescales (Section 4.2.3). Finally, we prepared regression models for these two first-order rate constants, and explored what the results imply about physical and biological controls on nitrate uptake across the LINX II sites (Section 4.2.4).

4.2.1. Transport Parameters at the LINX II Sites

Physical properties of the LINX II streams are highly variable both within and across the three land-use categories (Figures 5a–5f). Notably, reference streams have: (a) the highest median shear velocity, reflecting steeper slopes and more turbulent flows (Figures 5a and 5c); (b) the highest median Schmidt Number, reflecting cooler temperatures (Figures 5d and 5e); and (c) coarser sediment beds, reflecting the highest median d_{50} values (Figure 5f). The corresponding in-stream and in-bed mixing parameters k_m, $D_{\text{eff},0}$, and l_m (calculated from Equations 2a, 12a, and 13) also exhibit substantial variability within and across land-use categories (Figures 5g–5i). Remarkably, their median values all increase in the same order: agriculture streams ($10^{-3.8}$ ms^{-1}, $10^{-6.1}$ m^{2}s^{-1}, 2.5 mm) < urban streams ($10^{-3.7}$ ms^{-1}, $10^{-5.7}$ m^{2}s^{-1}, 5.0 mm) < reference streams ($10^{-3.6}$ ms^{-1}, $10^{-5.1}$ m^{2}s^{-1}, 8.0 mm). This land-use trend is consistent with previous studies on a subset of LINX II streams, which reported that streams draining urban and agricultural areas are geomorphically less complex, compared to reference streams, and consequently have less opportunity for exchange with both channel and subsurface storage zones (Crenshaw, 2010; Gooseff et al., 2007).

4.2.2. Inferred Reaction Rate Constants Across LINX II Sites

The resistor-in-series model for nitrate uptake (Equation 6) provides an explicit functional relationship between the nutrient uptake velocity in a stream (v_f), variables that characterize in-stream and in-bed mixing (k_m, $D_{\text{eff},0}$ and l_m), and the bulk first-order reaction rate constant for nutrient removal in the streambed (k) (see also Figure 1b). In the last section we presented estimates for the transport parameters (k_m, $D_{\text{eff},0}$ and l_m) at all LINX II sites. Further, the total and denitrification uptake velocities ($v_{f,\,tot}$ and $v_{f,\,den}$) were measured at these sites during LINX II. The first-order reaction rate constant is the only remaining unknown variable, and thus can be estimated for each LINX II stream by solving for k in Equation 6. Because k appears twice in this equation (once under the root and

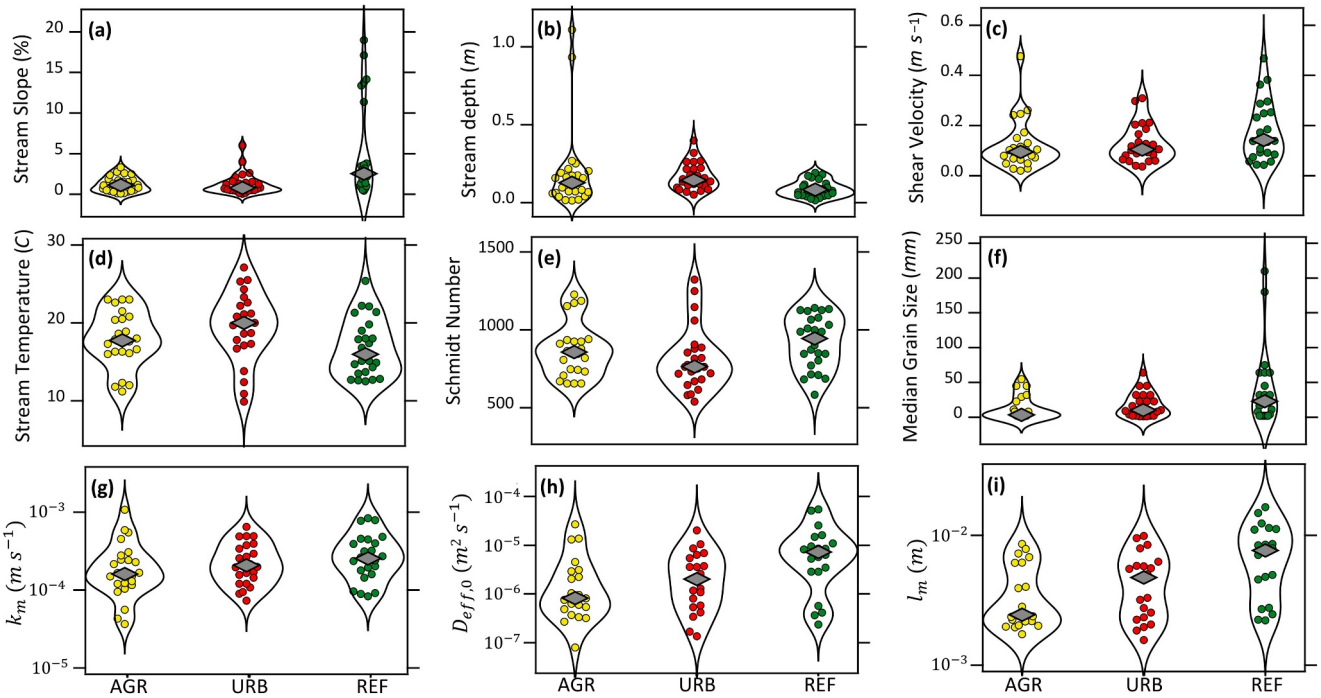

Figure 5. Measured and calculated variables for in-stream and in-bed mixing at the 72 LINX II headwater streams draining agricultural (AGR), urban (URB), and reference (REF) land-use types. (a–f) Site-specific values of: (a) measured stream slope, (b) measured stream depth, (c) calculated shear velocity, (d) measured stream temperature, (e) calculated Schmidt number, and (f) measured median grain size. (g–i) Estimates for in-stream and in-bed mixing parameters, including: (g) mass transfer coefficient (Equation 2a), (h) effective diffusivity at the sediment-water interface (Equation 12a), and (i) mixing depth scale (Equation 13).

also in the Damköhler Number), "solving for k" in this case involves numerically solving for the root of Equation 6 once all other variables have been defined.

Across the LINX II sites, nitrate uptake velocities for assimilation and denitrification ranged from $v_{f,\mathrm{tot}} \approx 10^{-6.4}$ to $10^{-3.8}$ m s^{-1} (Figure 6a) while those for denitrification alone ranged from $v_{f,\mathrm{den}} \approx 10^{-7.7}$ to $10^{-3.8}$ m s^{-1}

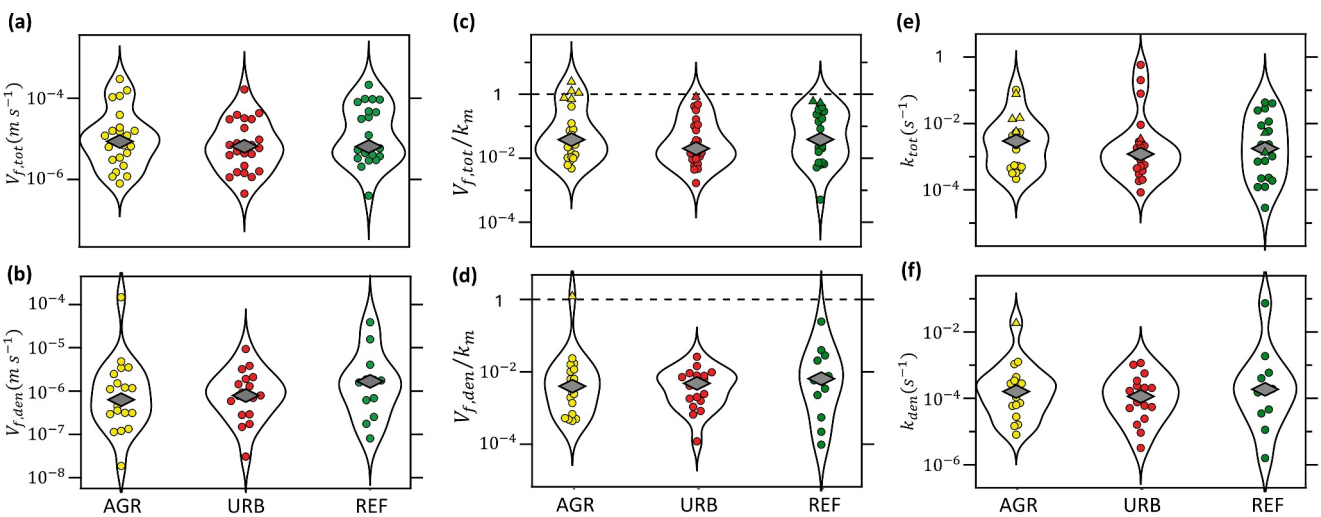

Figure 6. Previously published LINX II measurements of (a) total and (b) denitrification uptake velocities in streams draining agricultural (AGR), urban (URB), and reference (REF) land-use types. (c, d) When these measured uptake velocities are normalized by the convective mass transfer coefficient, k_m, the resulting ratios are generally less than unity (horizontal dashed line), consistent with the idea that in-stream mixing across the concentration boundary layer sets an upper limit on nitrate uptake. (e,f) Values of the in-sediment first-order reaction rate constants, k_{tot} and k_{den}, inferred from measurements of $v_{f,tot}$ and $v_{f,den}$ at the LINX II sites. Circles are rate constants inferred from Equation 6 and triangles are approximate lower limits (see main text).

(Figure 6b) (reproduced from Mulholland et al. (2008)). As noted by others (e.g., Plont et al. (2020)) median total and denitrification uptake velocities are relatively constant across land-use categories (Figures 6a and 6b). When these uptake velocities are normalized by their corresponding convective mass transfer coefficients the resulting ratios are generally less than unity, $v_f/k_m \leq 1$ (Figures 6c and 6d), consistent with a series arrangement of mass transfer resistances for in-stream and in-bed mixing (see Figure 2a and discussion thereof) and, more generally, the idea that convective mass transfer across the concentration boundary layer imposes an upper limit on the rate that nitrate can be removed by the streambed (Grant, Azizian, et al., 2018). Because the steady-state model assumes that the mass transfer coefficient imposes an upper limit on the uptake velocity, values of the first-order rate constant k inferred from Equation 6 will be poorly constrained as $v_f/k_m \to 1$. A lower-bound on the first-order rate constant can be calculated in this limit by noting that: (a) reaction rates are fast relative to transport rates, and therefore the Damköhler Number is likely to be large, $Da \gg 1$; (b) in the limit of large Damköhler Number, the second mass transfer resistor is approximately equal to, $R_2 \approx 1/\theta\sqrt{kD_{\text{eff},0}}$ (see Figure 2b and discussion thereof); and (c) substituting this last result into the inequality $R_2 < R_1 \approx 1/v_f$ yields the following lower-bound on the first-order rate constant, $k > v_f^2/\theta^2 D_{\text{eff},0}$. We used this lower-bound to estimate the first-order rate constant in all cases where $v_f/k_m \geq 0.5$ (triangles, Figures 6c–6f). In all other cases (i.e., for $v_f/k_m < 0.5$), first-order rate constants were inferred directly from Equation 6 (circles, Figures 6c–6f).

Inferred values of the first-order rate constant for total uptake or denitrification span similar ranges across the three land-use categories (Figures 6e and 6f). Median first-order rate constants for denitrification ($k_{den} = 10^{-3.8}$, $10^{-4.0}$, and $10^{-3.7}$ s^{-1} for agricultural, urban, and reference streams, respectively) are roughly an order of magnitude less than the first-order rate constants for total uptake ($k_{tot} = 10^{-2.5}$, $10^{-2.9}$, and $10^{-2.6}$ s^{-1}), reflecting the outsized role that assimilation (e.g., by autotrophs in the benthic biolayer, see Figure 1a) plays in nitrate uptake in these headwater streams.

4.2.3. In-Bed Reaction Timescales at the LINX II Sites

The corresponding reaction timescales, $\tau = 1/k$, range from 1.7 s to 9 hr ($10^{4.5}$ s) for total uptake and from 14 min ($10^{2.9}$ s) to 7.3 days ($10^{5.8}$ s) for denitrification (Figure 7a). These timescales are in line with previous reports of ca., 10 hr for denitrification in the hyporheic zone (Gomez-Velez et al., 2015) (black arrow labeled τ_{den}, Figure 7a) and $\approx 10^3$ to 10^7 s for oxygen consumption in the hyporheic zone (gray horizontal box, Figure 7a) (Gooseff et al., 2003); the timescale for oxygen consumption is relevant in this case because denitrification generally requires anoxic conditions to proceed (Alzate Marin et al., 2016; Rassamee et al., 2011; Zarnetske et al., 2011a).

As will be demonstrated in the next section, nitrate uptake at most LINX II sites is in the slow-reaction limit (i.e., $0 < Da \ll 1$). Under these conditions, the uptake velocity is linearly proportional to the first-order rate constant, $v_f \propto k$. By definition, the uptake velocity for assimilation is the difference between the total and denitrification uptake velocities, $v_{f,asm} = v_{f,tot} - v_{f,den}$ (Mulholland et al., 2008). Thus, when nitrate uptake is in the slow-reaction limit, the first-order rate constant for assimilation can be estimated from the difference in first-order rate constants for total uptake and denitrification, $k_{asm} = k_{tot} - k_{den}$; the corresponding assimilation reaction timescale is, $\tau_{asm} = (1/\tau_{tot} - 1/\tau_{den})^{-1}$. Assimilation timescales calculated using this approach are intermediate between those for total uptake and denitrification (median timescales for denitrification, assimilation, and total uptake are 1.8 hr, 26 and 8 min, respectively) (Figure 7a).

4.2.4. Regression Relationships for the Reaction Rate Constants

An MLR analysis of the inferred values for k_{tot} and k_{den} reveals that grain diameter d_{50}, stream nitrate concentration $\left[NO_3^-\right]$, GPP, and ER are all significant covariates (Figures 7b and 7c):

$$k_{tot} = 10^{-2.7\pm1.1} d_{50}^{-0.55\pm0.2} \left[NO_3^-\right]^{-0.6\pm0.1} \text{GPP}^{0.38\pm0.1},\ R^2 = 0.49 \tag{14a}$$

$$k_{den} = 10^{-0.69\pm1.5} d_{50}^{-0.49\pm0.14} \left[NO_3^-\right]^{-0.55\pm0.11} \text{ER}^{0.92\pm0.22},\ R^2 = 0.62 \tag{14b}$$

In this MLR study we allowed for two-way interaction effects, to account for the possibility that different relationships for k_{tot} and k_{den} might emerge for different land-use types. The fact that the two land-use variables (AGR(0, 1) and URB(0, 1), see Equations 10a and 10b) do not appear in Equations 14a and 14b implies that these

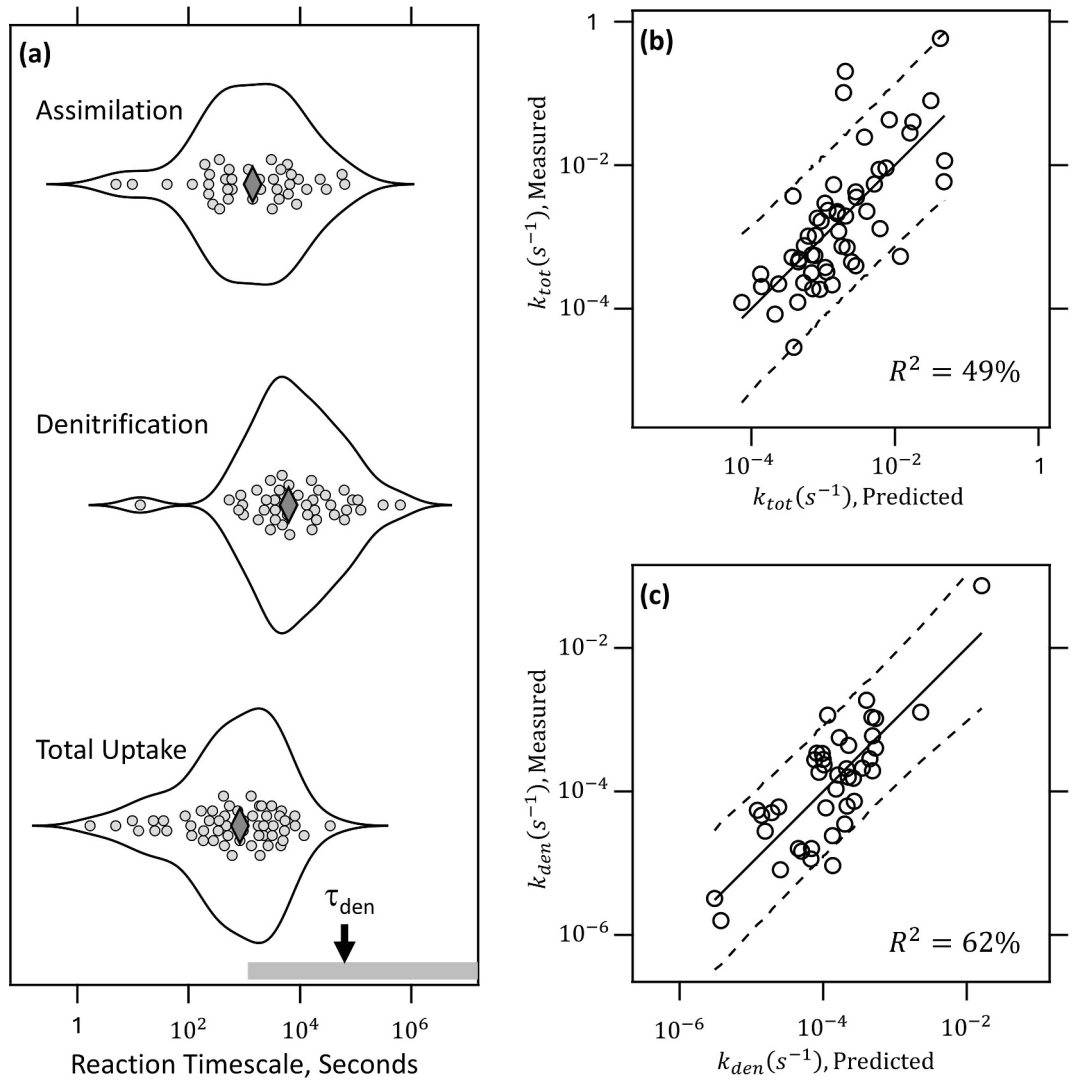

Figure 7. (a) Inferred reaction timescales for nitrate removal by both assimilation and denitrification ("Total Uptake"), denitrification alone ("Denitrification"), and assimilation alone ("Assimilation") (gray diamonds denote median values). Typical timescales for oxygen consumption (gray box) and denitrification (black arrow) in streambed sediments are also shown. (b and c) Performance of the top regression models for k_{tot} and k_{den} (see Equations 14a and 14b); solid line is a perfect correspondence, dashed lines are 90th percentile prediction intervals. The coefficient of determination for these relationships are also shown.

two regression equations are valid for all three land-use categories (recall that the influence of reference streams is implicitly represented by AGR(0, 1) = URB(0, 1) = 0). Also absent from these regression equations is the ratio of ER and GPP. This result is consistent with a previous assessment of the LINX II data set which found that organic carbon mineralization and nitrate uptake in these streams was not directly influenced by the ecosystem metabolic balance between GPP and ER (Plont et al., 2020). Although often correlated with stream metabolism (Lupon et al., 2016), stream temperature T is missing from our regression models either because it was not included in the top ranked model (for k_{tot}) or its regression coefficient was not significantly different than zero at $p < 0.01$ (for k_{den}). Both first-order rate constants depend inversely on median grain diameter d_{50} and the stream nitrate concentration $\left[NO_3^-\right]$ (Equations 14a and 14b). The former suggests that nitrate removal in the streambed proceeds more slowly in coarse sediments, perhaps due to the influence of specific surface area on microbial growth (Bailey & Ollis, 1986). The latter is a Monod-like biological saturation effect reported previously (Alexander et al., 2009; Bernot & Dodds, 2005; Dodds et al., 2002; Mulholland et al., 2008). Finally, the inclusion of GPP in Equation 14a is consistent with the contribution of nitrate assimilation by autotrophs to the magnitude

of k_{tot}, while the inclusion of ER in Equation 14b is consistent with the fact that denitrification generally requires anoxic conditions and therefore occurs more quickly in sediments with high rates of oxygen consumption (Mulholland et al., 2009; Thomas et al., 2001). Further, ER is often correlated with organic carbon availability, which can also be a limiting factor in measured denitrification rates (Plont et al., 2020; Zarnetske et al., 2011b).

4.2.5. Physical and Biological Controls on Nitrate Uptake

Across the headwater streams included in LINX II, most site-specific values of Da and N_R are less than unity (Figure S2 in Supporting Information S1), suggesting that: (a) reaction is slow relative to in-bed mixing and transport ($Da < 1$); (b) in-stream mixing is fast relative in-bed mixing and reaction ($N_R < 1$); and (c) mixing across the concentration boundary layer is fast relative to diffusive transport through the sediments ($Bi > 1$). Note that the first two conditions imply the third condition (see Equations 8a and 8b). For small Da and N_R our resistor-in-series model simplifies to, $v_f \approx \theta k l_m f(Da)$ where $f(Da) = -\gamma - \ln(Da)$ (Figure 2c). As noted earlier, in this slow-reaction limit, the hyporheic zone can be conceptualized as a well-mixed reactor; that is, the uptake velocity depends only on the first-order rate constant k and the volume per unit bed area of interstitial fluids, $\theta l_m f(Da)$. From the range of Da values estimated for the LINX II sites (Figure S2 in Supporting Information S1), the inferred reach-scale average effective depths of the hyporheic zone, $l_m f(Da)$, range from 0.1 mm to 10.3 cm for total nitrate uptake and 3 mm to 18 cm for denitrification alone.

From Equation 6 it can be shown that the slow-reaction limit applies, with less than 5% error, when $N_R < 1$ and $0 < Da < 0.01$; a condition that is met for a remarkable 48% of LINX II measurements of $v_{f,tot}$ and 90% of LINX II measurements of $v_{f,den}$ (Figure S2 in Supporting Information S1). In this limit the uptake velocity does not depend on the mass transfer coefficient, k_m, and only depends on the effective diffusivity at the sediment-water interface, $D_{\text{eff},0}$, to the extent that this parameter influences the depth of the mixing zone. Thus, another interpretation of the slow-reaction limit is that it corresponds to the asymptotic case where the uptake velocity is "biologically controlled"; that is, the uptake velocity is not rate-limited by physical transport across the concentration boundary layer nor by physical transport into the sediment bed by hyporheic zone mixing. Under this interpretation, the total uptake velocity is biologically controlled in nearly half of LINX II streams, while the rate of denitrification uptake is biologically controlled in nearly all LINX II streams. While consistent with previous assessments (Mulholland et al., 2008, 2009), it should be noted that this analysis is premised on a steady-state balance between areal flux and nitrate uptake in the streambed, a condition mimicked at LINX II sites by the continuous injection of ^{15}N labeled nitrate over a 24 hr period during summer baseflow conditions (Mulholland et al., 2008). If this balance is upset, for example, following a transient event like a storm or a spill, transport limitations cannot be ignored, even if the inequalities $N_R < 1$ and $0 < Da < 0.01$ are still satisfied.

The resistor-in-series model can also provide insights into which of the dimensionless variables introduced in this study (the resistor ratio N_R, the Damköhler Number Da, or the Biot Number Bi) exert the most influence on nitrate uptake velocities measured during LINX II. First we note that our resistor-in-series model for the uptake velocity can be written as a function of the resistor ratio alone: $v_f/k_m = N_R/(1 + N_R)$ (compare with Equation 6). The resistor ratio, in turn, is a composite dimensionless variable that incorporates all three physical and biological processes represented in the resistor-in-series model of the uptake velocity, including mixing across the concentration boundary layer, mixing into the sediment bed, and reaction in the sediment bed (see discussion of Steps 1, 2, and 3 in Figure 1b). The other two dimensionless variables are, in a sense, more fundamental, because they represent the balance between only two distinct processes; namely, rates of mixing across the concentration boundary layer and into the sediment bed (Bi) and rates of reaction and mixing within the sediment bed (Da). This explains why, as noted in Section 2.2, the resistor ratio can be written explicitly as a function of the other two dimensionless groups (see Equation 8a). Substituting Equation 8a into our expression above for the normalized uptake velocity we arrive at the following relationship between the normalized uptake velocity, the Damköhler Number, and the Biot Number:

$$\frac{v_f}{k_m} = \frac{\sqrt{Da}F(Da)/Bi}{1 + \sqrt{Da}F(Da)/Bi} \tag{15}$$

The Biot Number exhibits a relatively narrow range of values across the LINX II sites, from $Bi = 0.7$ to 3.2 (with a median of 1.4, results not shown). This observation, together with the nature of Equation 15, suggests that the

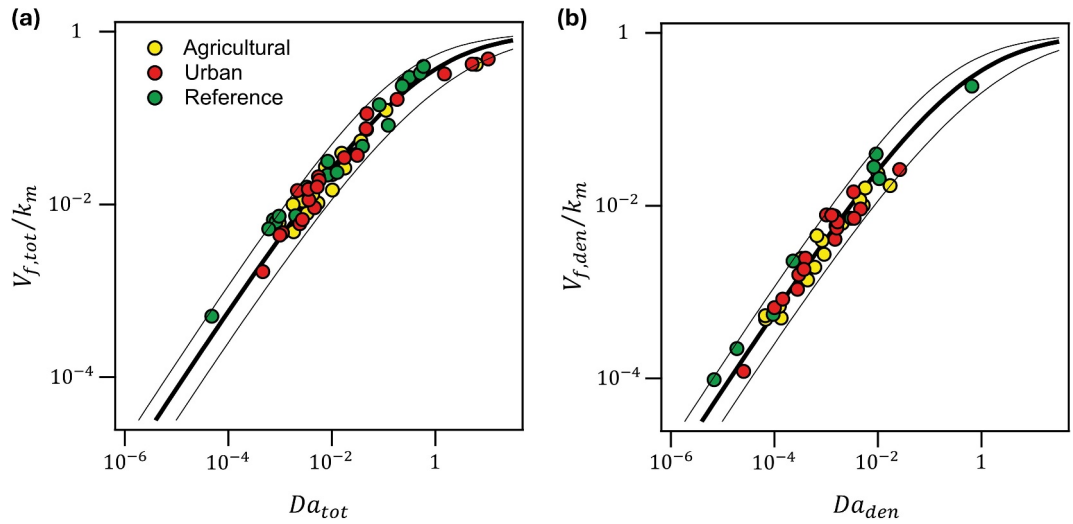

Figure 8. The Damköhler Number is a master variable for LINX II measurements of nitrate uptake in headwater streams, including the (a) total nitrate uptake velocity and (b) denitrification uptake velocity. Thick black curve is Equation 15 with the Biot Number set to the median value across all LINX II sites, $Bi = 1.4$. The upper and lower curves correspond to the extreme values, $Bi = 0.7$ and 3.2.

normalized uptake velocity may depend primarily on the Damköhler Number. Indeed, when plotted against the Damköhler Number, all of the normalized LINX II uptake velocities–including those for total uptake (Figure 8a) and denitrification alone (Figure 8b)–collapse onto a single curve. This single curve is well approximated by Equation 15 with the Biot Number set equal to its median value across the LINX II sites, $Bi = 1.4$ (thick solid line in Figures 8a and 8b); the upper and lower model curves correspond to the extreme values, Bi =0.7 and 3.2. The close concordance between measured and model-predicted LINX II uptake velocities is not surprising in and of itself; after all, the first-order rate constants for total uptake and denitrification were inferred directly from the resistor-in-series model, see Section 4.2.2. What is surprising, however, is that the measured uptake velocities track the model so closely for a single choice of the Biot Number, $Bi = 1.4$, and over a five order of magnitude change in the Damköhler number. Consistent with other reports of nutrient cycling in the hyporheic zone (Azizian et al., 2015, 2017; Boano et al., 2010; Kessler et al., 2013, 2015; Marzadri et al., 2011, 2014; Zarnetske et al., 2012, 2015), these results suggest that the Damköhler Number is a master variable for nitrate uptake across all of the LINX II sites.

5. Limitations and Future Research

The title of this paper suggests that our resistor-in-series model is a step toward a universal model for hyporheic exchange, but in its current form a number of limitations restrict its universal application. First, our evaluation of the two diffusivity depth profiles (C- or E-profiles) and the regression equations developed for $D_{\text{eff},0}$ and l_m (Equations 12a and 13) only capture those hyporheic exchange mechanisms represented among the 83 laboratory experiments included in the final MLR, including turbulent diffusion and dispersion across flat beds, bedform pumping across ripples and dunes, and larger-scale exchange processes associated with alternate bars. It remains to be seen if the simple modeling framework proposed here can be extended to additional hyporheic exchange mechanisms, in particular, and field measurements of hyporheic exchange, more generally. Additional hyporheic exchange mechanisms for which the current model could be evaluated include bedform migration (Shimony et al., 2023), stream meanders (Cardenas, 2009; Stonedahl et al., 2013), sediment heterogeneity (Liu et al., 2020; Su et al., 2020) and the flow obstructions commonly employed in stream restoration efforts (Hester & Gooseff, 2010, 2011).

Another potential limitation is the assumption that in-stream and in-bed mixing occur in series; that is, a pollutant molecule is first transported across the concentration boundary layer by stream turbulence, and then subsequently mixed into the streambed by one or more hyporheic exchange mechanisms. The sequential nature of these two mass transfer steps (see Figures 1b and 2a) is consistent with conventional theory (Thibodeaux et al., 2012),

laboratory flume experiments involving reactive sediment beds (O'Connor & Hondzo, 2008; O'Connor et al., 2009), and in situ and reach-scale measurements of nutrient uptake in streams (Anlanger et al., 2021). However, explicit evaluation of this assumption, particularly in contexts where stream turbulence penetrates into the streambed (e.g., under conditions of high permeability Reynolds Number (Roche et al., 2018)), is warranted.

Third, we tested the model using nitrate uptake velocities measured during LINX II, which included 72 headwater streams across eight regions of the US, collectively representing eight different biomes (temperate rain forest, chaparral, northern mixed forest, deciduous forest, montane, coniferous forest, temperate grassland, shrub desert and tropical forest) and three different land-use types (reference, urban, and agriculture). Notably, the model cannot be applied, in its current form, to larger (higher-order) streams in the river network where nitrogen processing and transformation may occur primarily in the water column and not in the benthic biolayer or hyporheic zone (Marzadri et al., 2017). However, in such cases our resistor-in-series model can be readily modified to include first-order reaction in the water column as an additional control on the uptake velocity.

Finally, our resistor-in-series model assumes that the streambed is infinitely deep. By comparing mixing parameters inferred from flume experiments using versions of the E-profile model that assume the hyporheic zone is either finite or infinite in extent, we find that the "infinite bed" approximation is valid so long as the bed depth is at least 30% the mixing length scale, $d_b/l_m > 0.3$. In situations where this inequality is not satisfied, the resistor-in-series model will need to be updated to explicitly account for the no-flux boundary condition at the bottom of the hyporheic zone.

6. Conclusions

While myriad physical and biological processes influence the rate of hyporheic exchange in a given setting, in this paper we demonstrate that several of the more ubiquitous exchange mechanisms can be represented simply as a one-dimensional diffusion process, where the diffusion coefficient, or effective diffusivity, decays exponentially with depth. We arrived at this conclusion by applying various analytical solutions of the unsteady one-dimensional diffusion equation to previously published laboratory measurements of hyporheic exchange. The analytical solutions take into account two-way feedback between solute concentrations in the sediment pore fluids and water column, and allow for a systematic exploration of the depth dependence of the diffusivity (constant or exponentially declining) and the nature of the bottom boundary (finite or infinite in extent).

Provided that the depth of the sediment bed, d_b, does not materially influence measured hyporheic exchange rates (i.e., the bed depth d_b is greater than 30% of the mixing depth, l_m, $d_b/l_m > 0.3$), we found that: (a) the exponential profile (E-profile) is superior to the constant profile (C-profile) based on model error (RMSE and NSE) and model parsimony (AICc); and (b) inferred values of the E-profile's two parameters (effective diffusivity at the sediment-water interface, $D_{\text{eff},0}$, and the length-scale over which the effective diffusivity decays with depth into the bed, l_m) are the same, within error, whether the analytical solution assumes that the sediment bed is finite (i.e., a no-flux boundary condition is imposed at the reported sediment depth, d_b) or infinite in extent. The E-profile model applies across a wide range of exchange mechanisms (including turbulent diffusion and dispersion across flat beds, advective pumping across ripples and dunes, and larger-scale exchange flows across alternate bars), experimental set-ups (recirculating flumes, stirred tanks, and once pass-through flumes), hydraulic conditions, and sediment bed properties. It also comports with previously published moment analyses of solute breakthrough curves measured in the field, which are consistent with a one-dimensional diffusive model of hyporheic zone mixing that declines exponentially with depth into the streambed (Bottacin-Busolin, 2017, 2019).

MLR studies of the E-profile's two parameters, $D_{\text{eff},0}$ and l_m, indicate that the former can be expressed as a power-law function of the permeability Reynolds Number, Re_K, and Schmidt Number, Sc (Equation 12a) while the latter can be expressed as a power-law function of the roughness Reynolds Number, Re_* and Schmidt Number (Equation 12b). Because the roughness Reynolds Number will be difficult to estimate in many settings, an alternative scaling expression for l_m was also developed based solely on Re_K and Sc (Equation 13). While this latter relationship explains slightly less variance, it improves the extensibility of our results by allowing both E-profile parameters to be calculated directly from Re_K and Sc. In turn, these two dimensionless variables can be estimated for a given stream from the median grain size of the sediment bed along with the stream's depth, slope, and temperature.

In the case of the effective diffusivity, the power-law exponent on the permeability Reynolds Number, Re_K^b, $b = 1.34 \pm 0.05$ (Equation 12a), is well within the range of previously reported values (1–2.5). In the case of the mixing length-scale, the power-law exponent on the permeability Reynolds Number, $b = 1.02 \pm 0.07$ (Equation 13), implies a direct proportionality with the permeability length-scale: $l_m \approx 16.6\sqrt{K}Sc^{0.44}$. When these power-law relationships for effective diffusivity and mixing length are applied to the 72 headwater streams included in LINX II, the results suggest substantial variability within and across land-use types. The median values of the effective diffusivity and mixing length-scale both increase in order agriculture < urban < reference, consistent with the idea that streams in urban and agricultural landscapes have lower geomorphic complexity and less opportunity for hyporheic exchange, relative to reference streams (Crenshaw, 2010; Gooseff et al., 2007).

The resistor-in-series model for nutrient uptake velocity can be used to infer first-order reaction rate constants for nitrate removal in the streambed from measured uptake velocities and regression equation estimates for the E-profile's mixing parameters, $D_{\text{eff},0}$ and l_m. When applied to the LINX II data set, we find that first-order rate constants for total uptake and denitrification uptake decrease with median grain diameter and stream nitrate concentration, but increase with either GPP (total uptake) or ER (denitrification uptake), consistent with previous assessments of the LINX II data set (Mulholland & Webster, 2010; Mulholland et al., 2008, 2009) (see Equations 14a and 14b). In turn, the inferred rate constants, along with regression estimates of the effective diffusivity and mixing length-scale, can be used to calculate site-specific values for the two key dimensionless variables Da and N_R. Across LINX II sites, the Biot Number varies by a factor of 4.6 (from 0.7 to 3.2), while the Damköhler Number varies by five orders of magnitude (from $10^{-4.3}$ to 10^{1} and from $10^{-5.2}$ to $10^{-0.2}$ for total and denitrification uptake, respectively). As a result, when the Biot Number is fixed at its median value (Bi =1.4), all of the LINX II uptake velocity measurements collapse onto a single curve when plotted against the Damköhler Number. This result is consistent with many other studies that suggest Da is a master variable for nitrate uptake in streams.

We show that reactive solute uptake by hyporheic exchange can be represented, both mathematically and conceptually, as two mass transfer resistors in series. The first resistor captures the in-stream mixing of solutes across the concentration boundary layer above the streambed. The second resistor captures in-bed mixing and first-order reaction of a reactive solute in the benthic biolayer and hyporheic zone. The classic transient storage model (which assumes that the hyporheic zone is a well-mixed reactor) is a special case of this more general resistor-in-series model, when the Biot Number and Damköhler Number are large and small, respectively.

The resistor-in-series model links together three disparate fields: (a) empirical field studies of reactive solute uptake in streams as quantified by the uptake velocity; (b) laboratory and multi-physics modeling studies of hyporheic exchange; and (c) the transformation of reactive solutes in the benthic biolayer and hyporheic zone by biological and abiotic processes. By "connecting the dots" across fields, the resistors-in-series model provides a common ground for analyzing diverse data sets.

For example, in this paper we combined LINX II field measurements of nitrate uptake in headwater streams with laboratory measurements and multi-physics modeling studies of hyporheic exchange to estimate first-order rate constants for nitrate removal in the benthic biolayer and hyporheic zone, from which site-specific Damköhler Numbers could be estimated. Looking forward, in a management context, the cross-disciplinary nature of the framework should prove useful for the design and evaluation of stream restoration projects, as many restorations aim to reduce streamborne pollution by increasing surface/subsurface exchange and harnessing in-bed biogeochemical reactions. The simplicity and extensibility of the framework should also inform reach-scale studies of pollutant fate and transport and facilitate their scale-up to watersheds and beyond.

Conflict of Interest

The authors declare no conflicts of interest relevant to this study.

Data Availability Statement

The data used and produced by the one-dimensional exponential diffusivity model for hyporheic exchange and nutrient cycling in streams can be access at Hydroshare (Monofy & Grant, 2024).

Acknowledgments
Funding was provided by U.S. National Science Foundation Growing Convergence Research Program (#2021015, #2020814, #2020820, #2312326), a Metropolitan Washington Council of Government award (#21-001), Virginia Tech College of Engineering Research Task Force project H2OStorm, Compagnia di San Paolo through the Joint Research Projects Initiative (project "RINSE - RIver Network SElf-depuration") and U.S. Department of Energy as part of the Watershed Dynamics and Evolution (WaDE) Science Focus Area at Oak Ridge National Laboratory and the IDEAS watersheds project, and by the project "Tracking Disturbance Signals Along River Networks" Laboratory Directed Research and Development Program of Oak Ridge National Laboratory, managed by UT-Battelle, LLC, for the U.S. Department of Energy.

References

Ahmerkamp, S., Winter, C., Janssen, F., Kuypers, M. M. M., & Holtappels, M. (2015). The impact of bedform migration on benthic oxygen fluxes. *Journal of Geophysical Research: Biogeosciences*, *120*(11), 2229–2242. https://doi.org/10.1002/2015JG003106

Akaike, H. (1974). A new look at the statistical model identification. *IEEE Transactions on Automatic Control*, *19*(6), 716–723. https://doi.org/10.1109/tac.1974.1100705

Alexander, R. B., Böhlke, J. K., Boyer, E. W., David, M. B., Harvey, J. W., Mulholland, P. J., et al. (2009). Dynamic modeling of nitrogen losses in river networks unravels the coupled effects of hydrological and biogeochemical processes. *Biogeochemistry*, *93*(1), 91–116. https://doi.org/10.1007/s10533-008-9274-8

Alkharusi, H. (2012). Categorical variables in regression analysis: A comparison of dummy and effect coding. *International Journal of Education*, *4*(2), 202. https://doi.org/10.5296/ije.v4i2.1962

Alzate Marin, J. C., Caravelli, A. H., & Zaritzky, N. E. (2016). Nitrification and aerobic denitrification in anoxic–aerobic sequencing batch reactor. *Bioresource Technology*, *200*, 380–387. https://doi.org/10.1016/j.biortech.2015.10.024

Anlanger, C., Risse-Buhl, U., von Schiller, D., Noss, C., Weitere, M., & Lorke, A. (2021). Hydraulic and biological controls of biofilm nitrogen uptake in gravel-bed streams. *Limnology and Oceanography*, *66*(11), 3887–3900. https://doi.org/10.1002/lno.11927

Azizian, M., Boano, F., Cook, P. L. M., Detwiler, R. L., Rippy, M. A., & Grant, S. B. (2017). Ambient groundwater flow diminishes nitrate processing in the hyporheic zone of streams. *Water Resources Research*, *53*(5), 3941–3967. https://doi.org/10.1002/2016WR020048

Azizian, M., Grant, S. B., Kessler, A. J., Cook, P. L. M., Rippy, M. A., & Stewardson, M. J. (2015). Bedforms as biocatalytic filters: A pumping and streamline segregation model for nitrate removal in permeable sediments. *Environmental Science & Technology*, *49*(18), 10993–11002. https://doi.org/10.1021/acs.est.5b01941

Bailey, J. E., & Ollis, D. F. (1986). *Biochemical engineering fundamentals*. (2nd ed.). McGraw-Hill.

Baxter, C. V., & Hauer, F. R. (2000). Geomorphology, hyporheic exchange, and selection of spawning habitat by bull trout (*Salvelinus confluentus*). *Canadian Journal of Fisheries and Aquatic Sciences*, *57*(7), 1470–1481. https://doi.org/10.1139/f00-056

Beaulieu, J. J., Tank, J. L., Hamilton, S. K., Wollheim, W. M., Hall, R. O., Mulholland, P. J., et al. (2011). Nitrous oxide emission from denitrification in stream and river networks. *Proceedings of the National Academy of Sciences*, *108*(1), 214–219. https://doi.org/10.1073/pnas.1011464108

Bencala, K. E. (2000). Hyporheic zone hydrological processes. *Hydrological Processes*, *14*(15), 2797–2798. https://doi.org/10.1002/1099-1085(20001030)14:15%3C2797::AID-HYP402%3E3.0.CO;2-6

Bernot, M. J., & Dodds, W. K. (2005). Nitrogen retention, removal, and saturation in lotic ecosystems. *Ecosystems*, *8*(4), 442–453. https://doi.org/10.1007/s10021-003-0143-y

Bhattarai, B., Hilliard, B., Reeder, W. J., Budwig, R., Martin, B. T., Xing, T., & Tonina, D. (2023). Effect of surface hydraulics and salmon redd size on redd-induced hyporheic exchange. *Water Resources Research*, *59*(6), e2022WR033977. https://doi.org/10.1029/2022WR033977

Boano, F., Demaria, A., Revelli, R., & Ridolfi, L. (2010). Biogeochemical zonation due to intrameander hyporheic flow. *Water Resources Research*, *46*(2), W02511. https://doi.org/10.1029/2008WR007583

Boano, F., Harvey, J. W., Marion, A., Packman, A. I., Revelli, R., Ridolfi, L., & Wörman, A. (2014). Hyporheic flow and transport processes: Mechanisms, models, and biogeochemical implications. *Reviews of Geophysics*, *52*(4), 603–679. https://doi.org/10.1002/2012RG000417

Boano, F., Revelli, R., & Ridolfi, L. (2013). Modeling hyporheic exchange with unsteady stream discharge and bedform dynamics. *Water Resources Research*, *49*(7), 4089–4099. https://doi.org/10.1002/wrcr.20322

Bottacin-Busolin, A. (2017). Non-Fickian dispersion in open-channel flow over a porous bed. *Water Resources Research*, *53*(8), 7426–7456. https://doi.org/10.1002/2016WR020348

Bottacin-Busolin, A. (2019). Modeling the effect of hyporheic mixing on stream solute transport. *Water Resources Research*, *55*(11), 9995–10011. https://doi.org/10.1029/2019WR025697

Boulton, A. J., Datry, T., Kasahara, T., Mutz, M., & Stanford, J. A. (2010). Ecology and management of the hyporheic zone: Stream–groundwater interactions of running waters and their floodplains. *Journal of the North American Benthological Society*, *29*(1), 26–40. https://doi.org/10.1899/08-017.1

Brewer, M. J., Butler, A., & Cooksley, S. L. (2016). The relative performance of AIC, AICC and BIC in the presence of unobserved heterogeneity. *Methods in Ecology and Evolution*, *7*(6), 679–692. https://doi.org/10.1111/2041-210X.12541

Buckingham, E. (1914). On physically similar systems; illustrations of the use of dimensional equations. *Physical Review*, *4*(4), 345–376. https://doi.org/10.1103/PhysRev.4.345

Calcagno, V., & Mazancourt, C. D. (2010). glmulti: An R package for easy automated model selection with (generalized) linear models. *Journal of Statistical Software*, *34*(12), 1–29. https://doi.org/10.18637/jss.v034.i12

Cardenas, M. B. (2009). Stream-aquifer interactions and hyporheic exchange in gaining and losing sinuous streams. *Water Resources Research*, *45*(6), W06429. https://doi.org/10.1029/2008WR007651

Cardenas, M. B. (2015). Hyporheic zone hydrologic science: A historical account of its emergence and a prospectus. *Water Resources Research*, *51*(5), 3601–3616. https://doi.org/10.1002/2015WR017028

Cardenas, M. B., Wilson, J. L., & Haggerty, R. (2008). Residence time of bedform-driven hyporheic exchange. *Advances in Water Resources*, *31*(10), 1382–1386. https://doi.org/10.1016/j.advwatres.2008.07.006

Chandler, I. D., Guymer, I., Pearson, J. M., & Van Egmond, R. (2016). Vertical variation of mixing within porous sediment beds below turbulent flows. *Water Resources Research*, *52*(5), 3493–3509. https://doi.org/10.1002/2015WR018274

Chen, C. Y., Fytanidis, D. K., & Garcia, M. H. (2024). A unifying model for turbulent hyporheic mass flux under a wide range of near-bed hydrodynamic conditions. *Geophysical Research Letters*, *51*(6), e2023GL105807. https://doi.org/10.1029/2023GL105807

Chen, Y., Jin, G., Zhang, P., Jiang, Q., Wu, S., Galindo Torres, S. A., & Li, L. (2021). A pore-scale study of flow and transport across the sediment–water interface: From dispersive to turbulent regimes. *Physics of Fluids*, *33*(12), 126601. https://doi.org/10.1063/5.0064350

Coll, C., Bier, R., Li, Z., Langenheder, S., Gorokhova, E., & Sobek, A. (2020). Association between aquatic micropollutant dissipation and river sediment bacterial communities. *Environmental Science & Technology*, *54*(22), 14380–14392. https://doi.org/10.1021/acs.est.0c04393

Crenshaw, C. G. (2010). Dissolved inorganic nitrogen dynamics in the hyporheic zone of reference and human-altered southwestern U. S. streams. *Fundamental and Applied Limnology*, *176*(4), 391–405. https://doi.org/10.1127/1863-9135/2010/0176-0391

Dodds, W. K., Smith, V. H., & Lohman, K. (2002). Nitrogen and phosphorus relationships to benthic algal biomass in temperate streams. *Canadian Journal of Fisheries and Aquatic Sciences*, *59*(5), 865–874. https://doi.org/10.1139/f02-063

Elliott, A. H. (1991). *Transfer of solutes into and out of streambeds* (PhD). California Institute of Technology. Retrieved from https://resolver.caltech.edu/CaltechETD:etd-07092007-074127

Elliott, A. H., & Brooks, N. H. (1997a). Transfer of nonsorbing solutes to a streambed with bed forms: Laboratory experiments. *Water Resources Research*, *33*(1), 137–151. https://doi.org/10.1029/96WR02783

Elliott, A. H., & Brooks, N. H. (1997b). Transfer of nonsorbing solutes to a streambed with bed forms: Theory. *Water Resources Research*, *33*(1), 123–136. https://doi.org/10.1029/96WR02784

Eylers, H. (1994). *Transport of adsorbing metal ions between stream water and sediment bed in a laboratory flume* (Unpublished doctoral dissertation). Caltech.

Fellows, C. S., Valett, H. M., Dahm, C. N., Mulholland, P. J., & Thomas, S. A. (2006). Coupling nutrient uptake and energy flow in headwater streams. *Ecosystems*, *9*(5), 788–804. https://doi.org/10.1007/s10021-006-0005-5

Gomez-Velez, J. D., Harvey, J. W., Cardenas, M. B., & Kiel, B. (2015). Denitrification in the Mississippi River network controlled by flow through river bedforms. *Nature Geoscience*, *8*(12), 941–945. https://doi.org/10.1038/ngeo2567

Gomez-Velez, J. D., Krause, S., & Wilson, J. L. (2014). Effect of low-permeability layers on spatial patterns of hyporheic exchange and groundwater upwelling. *Water Resources Research*, *50*(6), 5196–5215. https://doi.org/10.1002/2013WR015054

González-Pinzón, R., Haggerty, R., & Dentz, M. (2013). Scaling and predicting solute transport processes in streams. *Water Resources Research*, *49*(7), 4071–4088. https://doi.org/10.1002/wrcr.20280

Gooseff, M. N. (2010). Defining hyporheic zones – Advancing our conceptual and operational definitions of where stream water and groundwater meet. *Geography Compass*, *4*(8), 945–955. https://doi.org/10.1111/j.1749-8198.2010.00364.x

Gooseff, M. N., Hall, R. O., Jr., & Tank, J. L. (2007). Relating transient storage to channel complexity in streams of varying land use in Jackson Hole, Wyoming. *Water Resources Research*, *43*(1), W01417. https://doi.org/10.1029/2005WR004626

Gooseff, M. N., Wondzell, S. M., Haggerty, R., & Anderson, J. (2003). Comparing transient storage modeling and residence time distribution (RTD) analysis in geomorphically varied reaches in the Lookout Creek basin, Oregon, USA. *Advances in Water Resources*, *26*(9), 925–937. https://doi.org/10.1016/S0309-1708(03)00105-2

Grant, S. B., Azizian, M., Cook, P., Boano, F., & Rippy, M. A. (2018). Factoring stream turbulence into global assessments of nitrogen pollution. *Science*, *359*(6381), 1266–1269. https://doi.org/10.1126/science.aap8074

Grant, S. B., Gomez-Velez, J. D., & Ghisalberti, M. (2018). Modeling the effects of turbulence on hyporheic exchange and local-to-global nutrient processing in streams. *Water Resources Research*, *54*(9), 5883–5889. https://doi.org/10.1029/2018WR023078

Grant, S. B., Gomez-Velez, J. D., Ghisalberti, M., Guymer, I., Boano, F., Roche, K., & Harvey, J. (2020). A one-dimensional model for turbulent mixing in the benthic biolayer of stream and coastal sediments. *Water Resources Research*, *56*(12), e2019WR026822. https://doi.org/10.1029/2019WR026822

Grant, S. B., & Marusic, I. (2011). Crossing turbulent boundaries: Interfacial flux in environmental flows. *Environmental Science & Technology*, *45*(17), 7107–7113. https://doi.org/10.1021/es201778s

Grant, S. B., Monofy, A., Boano, F., Gomez-Velez, J. D., Guymer, I., Harvey, J., & Ghisalberti, M. (2020). Unifying advective and diffusive descriptions of bedform pumping in the benthic biolayer of streams. *Water Resources Research*, *56*(11), e2020WR027967. https://doi.org/10.1029/2020WR027967

Grant, S. B., Stewardson, M. J., & Marusic, I. (2012). Effective diffusivity and mass flux across the sediment-water interface in streams. *Water Resources Research*, *48*(5), W05548. https://doi.org/10.1029/2011WR011148

Hall, R. O., Tank, J. L., Sobota, D. J., Mulholland, P. J., O'Brien, J. M., Dodds, W. K., et al. (2009). Nitrate removal in stream ecosystems measured by ^{15}N addition experiments: Total uptake. *Limnology and Oceanography*, *54*(3), 653–665. https://doi.org/10.4319/lo.2009.54.3.0653

Hester, E. T., Cardenas, M. B., Haggerty, R., & Apte, S. V. (2017). The importance and challenge of hyporheic mixing. *Water Resources Research*, *53*(5), 3565–3575. https://doi.org/10.1002/2016WR020005

Hester, E. T., & Gooseff, M. N. (2010). Moving beyond the banks: Hyporheic restoration is fundamental to restoring ecological services and functions of streams. *Environmental Science & Technology*, *44*(5), 1521–1525. https://doi.org/10.1021/es902988n

Hester, E. T., & Gooseff, M. N. (2011). Hyporheic restoration in streams and rivers. In *Stream restoration in dynamic fluvial systems* (pp. 167–187). American Geophysical Union (AGU). https://doi.org/10.1029/2010GM000966

Hester, E. T., Young, K. I., & Widdowson, M. A. (2013). Mixing of surface and groundwater induced by riverbed dunes: Implications for hyporheic zone definitions and pollutant reactions. *Water Resources Research*, *49*(9), 5221–5237. https://doi.org/10.1002/wrcr.20399

Huang, S. H., & Yang, J. Q. (2023). Impacts of channel-spanning log jams on hyporheic flow. *Water Resources Research*, *59*(11), e2023WR035217. https://doi.org/10.1029/2023WR035217

Kessler, A. J., Cardenas, M. B., & Cook, P. L. M. (2015). The negligible effect of bed form migration on denitrification in hyporheic zones of permeable sediments. *Journal of Geophysical Research: Biogeosciences*, *120*(3), 538–548. https://doi.org/10.1002/2014JG002852

Kessler, A. J., Glud, R. N., Cardenas, M. B., & Cook, P. L. M. (2013). Transport zonation limits coupled nitrification-denitrification in permeable sediments. *Environmental Science & Technology*, *47*(23), 13404–13411. https://doi.org/10.1021/es403318x

Knapp, J. L., & Kelleher, C. (2020). A perspective on the future of transient storage modeling: Let's stop chasing our tails. *Water Resources Research*, *56*(3), e2019WR026257. https://doi.org/10.1029/2019WR026257

Krause, S., Abbott, B. W., Baranov, V., Bernal, S., Blaen, P., Datry, T., et al. (2022). Organizational principles of hyporheic exchange flow and biogeochemical cycling in river networks across scales. *Water Resources Research*, *58*(3), e2021WR029771. https://doi.org/10.1029/2021WR029771

Krause, S., Hannah, D. M., Fleckenstein, J. H., Heppell, C. M., Kaeser, D., Pickup, R., et al. (2011). Inter-disciplinary perspectives on processes in the hyporheic zone. *Ecohydrology*, *4*(4), 481–499. https://doi.org/10.1002/eco.176

Lai, J. L., Lo, S. L., & Lin, C. F. (1994). Effects of hydraulic and medium characteristics on solute transfer to surface runoff. *Water Science and Technology*, *30*(7), 145–155. https://doi.org/10.2166/wst.1994.0329

Lewandowski, J., Arnon, S., Banks, E., Batelaan, O., Betterle, A., Broecker, T., et al. (2019). Is the hyporheic zone relevant beyond the scientific community? *Water*, *11*(11), 2230. https://doi.org/10.3390/w11112230

Liu, Y., Reible, D., & Hussain, F. (2022). Roles of tidal cycling, hyporheic exchange and bioirrigation on metal release from estuary sediments. *Water Resources Research*, *58*(4), e2021WR030790. https://doi.org/10.1029/2021WR030790

Liu, Y., Wallace, C. D., Zhou, Y., Ershadnia, R., Behzadi, F., Dwivedi, D., et al. (2020). Influence of streambed heterogeneity on hyporheic flow and sorptive solute transport. *Water*, *12*(6), 1547. https://doi.org/10.3390/w12061547

Lupon, A., Martí, E., Sabater, F., & Bernal, S. (2016). Green light: Gross primary production influences seasonal stream N export by controlling fine-scale N dynamics. *Ecology*, *97*(1), 133–144. https://doi.org/10.1890/14-2296.1

Marion, A., & Zaramella, M. (2005). Diffusive behavior of bedform-induced hyporheic exchange in rivers. *Journal of Environmental Engineering*, *131*(9), 1260–1266. https://doi.org/10.1061/(ASCE)0733-9372(2005)131:9(1260)

Marzadri, A., Dee, M. M., Tonina, D., Bellin, A., & Tank, J. L. (2017). Role of surface and subsurface processes in scaling N_2O emissions along riverine networks. *Proceedings of the National Academy of Sciences*, *114*(17), 4330–4335. https://doi.org/10.1073/pnas.1617454114

Marzadri, A., Tonina, D., & Bellin, A. (2011). A semianalytical three-dimensional process-based model for hyporheic nitrogen dynamics in gravel bed rivers. *Water Resources Research*, *47*(11), W11518. https://doi.org/10.1029/2011WR010583

Marzadri, A., Tonina, D., Bellin, A., & Tank, J. L. (2014). A hydrologic model demonstrates nitrous oxide emissions depend on streambed morphology. *Geophysical Research Letters*, *41*(15), 5484–5491. https://doi.org/10.1002/2014GL060732

Monofy, A., & Boano, F. (2021). The effect of streamflow, ambient groundwater, and sediment anisotropy on hyporheic zone characteristics in alternate bars. *Water Resources Research*, *57*(1), e2019WR025069. https://doi.org/10.1029/2019WR025069

Monofy, A., & Grant, S. (2024). Data for a manuscript titled, "Toward a universal model of hyporheic exchange and nutrient cycling in streams" [Dataset]. *HydroShare*. http://www.hydroshare.org/resource/9c63193bea2943d08f962576613b57c9

Mulholland, P. J., Hall, R. O., Jr., Sobota, D. J., Dodds, W. K., Findlay, S. E. G., Grimm, N. B., et al. (2009). Nitrate removal in stream ecosystems measured by ^{15}N addition experiments: Denitrification. *Limnology and Oceanography*, *54*(3), 666–680. https://doi.org/10.4319/lo.2009.54.3.0666

Mulholland, P. J., Helton, A. M., Poole, G. C., Hall, R. O., Hamilton, S. K., Peterson, B. J., et al. (2008). Stream denitrification across biomes and its response to anthropogenic nitrate loading. *Nature*, *452*(7184), 202–205. https://doi.org/10.1038/nature06686

Mulholland, P. J., & Webster, J. R. (2010). Nutrient dynamics in streams and the role of J-NABS. *Journal of the North American Benthological Society*, *29*(1), 100–117. https://doi.org/10.1899/08-035.1

Newbold, J. D., Elwood, J. W., O'Neill, R. V., & Winkle, W. V. (1981). Measuring nutrient spiralling in streams. *Canadian Journal of Fisheries and Aquatic Sciences*, *38*(7), 860–863. https://doi.org/10.1139/f81-114

O'Brien, J. M., & Dodds, W. K. (2010). Saturation of NO_3^- uptake in prairie streams as a function of acute and chronic N exposure. *Journal of the North American Benthological Society*, *29*(2), 627–635. https://doi.org/10.1899/09-021.1

O'Connor, B. L., & Harvey, J. W. (2008). Scaling hyporheic exchange and its influence on biogeochemical reactions in aquatic ecosystems. *Water Resources Research*, *44*(12), W12423. https://doi.org/10.1029/2008WR007160

O'Connor, B. L., & Hondzo, M. (2008). Dissolved oxygen transfer to sediments by sweep and eject motions in aquatic environments. *Limnology and Oceanography*, *53*(2), 566–578. https://doi.org/10.4319/lo.2008.53.2.0566

O'Connor, B. L., Hondzo, M., & Harvey, J. W. (2009). Incorporating both physical and kinetic limitations in quantifying dissolved oxygen flux to aquatic sediments. *Journal of Environmental Engineering*, *135*(12), 1304–1314. https://doi.org/10.1061/(ASCE)EE.1943-7870.0000093

Ott, L., & Longnecker, M. (2004). *A first course in statistical methods*. Thomson-Brooks/Cole.

Packman, A. I., Brooks, N. H., & Morgan, J. J. (2000). Kaolinite exchange between a stream and streambed: Laboratory experiments and validation of a colloid transport model. *Water Resources Research*, *36*(8), 2363–2372. https://doi.org/10.1029/2000WR900058

Packman, A. I., & MacKay, J. S. (2003). Interplay of stream-subsurface exchange, clay particle deposition, and streambed evolution. *Water Resources Research*, *39*(4), 1097. https://doi.org/10.1029/2002WR001432

Packman, A. I., Salehin, M., & Zaramella, M. (2004). Hyporheic exchange with gravel beds: Basic hydrodynamic interactions and bedform-induced advective flows. *Journal of Hydraulic Engineering*, *130*(7), 647–656. https://doi.org/10.1061/(ASCE)0733-9429(2004)130:7(647)

Ping, X., Xian, Y., & Jin, M. (2022). Influence of bedform migration on nitrate reduction in hyporheic zones of heterogeneous sediments. *Water Resources Research*, *58*(11), e2022WR033258. https://doi.org/10.1029/2022WR033258

Plont, S., O'Donnell, B. M., Gallagher, M. T., & Hotchkiss, E. R. (2020). Linking carbon and nitrogen spiraling in streams. *Freshwater Science*, *39*(1), 126–136. https://doi.org/10.1086/707810

Rassamee, V., Sattayatewa, C., Pagilla, K., & Chandran, K. (2011). Effect of oxic and anoxic conditions on nitrous oxide emissions from nitrification and denitrification processes. *Biotechnology and Bioengineering*, *108*(9), 2036–2045. https://doi.org/10.1002/bit.23147

Rehg, K. J., Packman, A. I., & Ren, J. (2005). Effects of suspended sediment characteristics and bed sediment transport on streambed clogging. *Hydrological Processes*, *19*(2), 413–427. https://doi.org/10.1002/hyp.5540

Ren, J., Hu, H., Lu, X., & Yu, R. (2023). Water and heat exchange responses to flooding and local storm events in the hyporheic zone driven by a meandering bend. *Science of the Total Environment*, *883*, 163732. https://doi.org/10.1016/j.scitotenv.2023.163732

Richardson, C. P., & Parr, A. D. (1988). Modified Fickian model for solute uptake by runoff. *Journal of Environmental Engineering*, *114*(4), 792–809. https://doi.org/10.1061/(ASCE)0733-9372(1988)114:4(792)

Roche, K. R., Blois, G., Best, J. L., Christensen, K. T., Aubeneau, A. F., & Packman, A. I. (2018). Turbulence links momentum and solute exchange in coarse-grained streambeds. *Water Resources Research*, *54*(5), 3225–3242. https://doi.org/10.1029/2017WR021992

Roche, K. R., Li, A., Bolster, D., Wagner, G. J., & Packman, A. I. (2019). Effects of turbulent hyporheic mixing on reach-scale transport. *Water Resources Research*, *55*(5), 3780–3795. https://doi.org/10.1029/2018WR023421

Runkel, R. L. (2007). Toward a transport-based analysis of nutrient spiraling and uptake in streams. *Limnology and Oceanography: Methods*, *5*(1), 50–62. https://doi.org/10.4319/lom.2007.5.50

Salarashayeri, A. F., & Siosemarde, M. (2012). Prediction of soil hydraulic conductivity from particle-size distribution. *International Journal of Geological and Environmental Engineering*, *6*(1), 16–20.

Sawyer, A. H., Bayani Cardenas, M., & Buttles, J. (2011). Hyporheic exchange due to channel-spanning logs. *Water Resources Research*, *47*(8), W08502. https://doi.org/10.1029/2011WR010484

Shimony, T., Teitelbaum, Y., Cifuentes, E. S., Dallmann, J., Phillips, C. B., Packman, A. I., & Arnon, S. (2023). Kaolinite deposition dynamics and streambed clogging during bedform migration under losing and gaining flow conditions. *Water Resources Research*, *59*(9), e2023WR034792. https://doi.org/10.1029/2023WR034792

Shrivastava, S., Stewardson, M. J., & Arora, M. (2021). Influence of bioturbation on hyporheic exchange in streams: Conceptual model and insights from laboratory experiments. *Water Resources Research*, *57*(2), e2020WR028468. https://doi.org/10.1029/2020WR028468

Stonedahl, S. H., Harvey, J. W., & Packman, A. I. (2013). Interactions between hyporheic flow produced by stream meanders, bars, and dunes. *Water Resources Research*, *49*(9), 5450–5461. https://doi.org/10.1002/wrcr.20400

Stream Solute Workshop. (1990). Concepts and methods for assessing solute dynamics in stream ecosystems. *Journal of the North American Benthological Society*, *9*(2), 95–119. https://doi.org/10.2307/1467445

Su, X., Jim Yeh, T.-C., Shu, L., Li, K., Brusseau, M. L., Wang, W., et al. (2020). Scale issues and the effects of heterogeneity on the dune-induced hyporheic mixing. *Journal of Hydrology*, *590*, 125429. https://doi.org/10.1016/j.jhydrol.2020.125429

Su, X., Yeh, T.-C. J., Li, K., Wang, G., Wang, W., & Hao, Y. (2024). The impact of heterogeneity at various spatial locations on dune-induced hyporheic exchange. *Journal of Hydrology*, *629*, 130526. https://doi.org/10.1016/j.jhydrol.2023.130526

Thibodeaux, L., Valsaraj, K., & Reible, D. (2012). Letter to the editor regarding, "Crossing turbulent boundaries: Interfacial flux in environment flows". *Environmental Science & Technology*, *46*(3), 1293–1294. https://doi.org/10.1021/es300040t

Thomas, S., Valett, H., Mulholland, P., Fellows, C., Webster, J., Dahm, C., & Peterson, C. (2001). Nitrogen retention in headwater streams: The influence of groundwater-surface water exchange. *The Scientific World Journal*, *1*(2), 623–631. https://doi.org/10.1100/tsw.2001.272

Tonina, D., & Buffington, J. M. (2007). Hyporheic exchange in gravel bed rivers with pool-riffle morphology: Laboratory experiments and three-dimensional modeling. *Water Resources Research*, *43*(1), W01421. https://doi.org/10.1029/2005WR004328

Trauth, N., Schmidt, C., Maier, U., Vieweg, M., & Fleckenstein, J. H. (2013). Coupled 3-D stream flow and hyporheic flow model under varying stream and ambient groundwater flow conditions in a pool-riffle system. *Water Resources Research*, *49*(9), 5834–5850. https://doi.org/10.1002/wrcr.20442

Voermans, J. J., Ghisalberti, M., & Ivey, G. N. (2017). The variation of flow and turbulence across the sediment–water interface. *Journal of Fluid Mechanics*, *824*, 413–437. https://doi.org/10.1017/jfm.2017.345

Voermans, J. J., Ghisalberti, M., & Ivey, G. N. (2018). A model for mass transport across the sediment-water interface. *Water Resources Research*, *54*(4), 2799–2812. https://doi.org/10.1002/2017WR022418

Ward, A. S., Schmadel, N. M., Wondzell, S. M., Harman, C., Gooseff, M. N., & Singha, K. (2016). Hydrogeomorphic controls on hyporheic and riparian transport in two headwater mountain streams during base flow recession. *Water Resources Research*, *52*(2), 1479–1497. https://doi.org/10.1002/2015WR018225

Webster, J. R., Mulholland, P. J., Tank, J. L., Valett, H. M., Dodds, W. K., Peterson, B. J., et al. (2003). Factors affecting ammonium uptake in streams – An inter-biome perspective. *Freshwater Biology*, *48*(8), 1329–1352. https://doi.org/10.1046/j.1365-2427.2003.01094.x

Webster, J. R., & Patten, B. C. (1979). Effects of watershed perturbation on stream potassium and calcium dynamics. *Ecological Monographs*, *49*(1), 51–72. https://doi.org/10.2307/1942572

Weglarczyk, S. (1998). The interdependence and applicability of some statistical quality measures for hydrological models. *Journal of Hydrology*, *206*(1–2), 98–103. https://doi.org/10.1016/S0022-1694(98)00094-8

Wymore, A. S., Rodríguez-Cardona, B. M., Herreid, A., & McDowell, W. H. (2019). LINX I and II: Lessons learned and emerging questions. *Frontiers in Environmental Science*, *7*, 181. https://doi.org/10.3389/fenvs.2019.00181

Zarnetske, J. P., Haggerty, R., & Wondzell, S. M. (2015). Coupling multiscale observations to evaluate hyporheic nitrate removal at the reach scale. *Freshwater Science*, *34*(1), 172–186. https://doi.org/10.1086/680011

Zarnetske, J. P., Haggerty, R., Wondzell, S. M., & Baker, M. A. (2011a). Dynamics of nitrate production and removal as a function of residence time in the hyporheic zone. *Journal of Geophysical Research*, *116*(G1), G01025. https://doi.org/10.1029/2010JG001356

Zarnetske, J. P., Haggerty, R., Wondzell, S. M., & Baker, M. A. (2011b). Labile dissolved organic carbon supply limits hyporheic denitrification. *Journal of Geophysical Research*, *116*(G4), G04036. https://doi.org/10.1029/2011JG001730

Zarnetske, J. P., Haggerty, R., Wondzell, S. M., Bokil, V. A., & González-Pinzón, R. (2012). Coupled transport and reaction kinetics control the nitrate source-sink function of hyporheic zones. *Water Resources Research*, *48*(11), W11508. https://doi.org/10.1029/2012WR011894

References From the Supporting Information

Ren, J., & Packman, A. I. (2004). Stream-subsurface exchange of zinc in the presence of silica and kaolinite colloids. *Environmental Science & Technology*, *38*(24), 6571–6581. https://doi.org/10.1021/es035090x

Yates, S. R. (1992). An analytical solution for one-dimensional transport in porous media with an exponential dispersion function. *Water Resources Research*, *28*(8), 2149–2154. https://doi.org/10.1029/92WR01006